AD NUMBER
AD041743
CLASSIFICATION CHANGES
TO: **unclassified**
FROM: **confidential**
LIMITATION CHANGES
TO: **Approved for public release; distribution is unlimited.**
FROM: **Distribution authorized to DoD only; Administrative/Operational Use; MAR 1952. Other requests shall be referred to Naval Air Systems Command, Washington, DC 20362. Pre-dates formal DoD distribution statements. Treat as DoD only.**
AUTHORITY
31 Mar 1964, DoDD 5200.10; APL ltr dtd 11 Mar 1967 per Navy

AD

41743

CONFIDENTIAL

RAMJET TECHNOLOGY

AFL/JHU TG 154-7

Chapter 7

AIR-FUEL MIXTURE PREPARATION

by

J. P. LONGWELL
and
M. A. WEISS

Standard Oil Development Company
ESSO Laboratories

Published by

THE JOHNS HOPKINS UNIVERSITY
APPLIED PHYSICS LABORATORY
Silver Spring **Maryland**

Operating under Contract NOrd 7386 with
the Bureau of Ordnance, Department of the Navy

Chapter 7

AIR-FUEL MIXTURE PREPARATION

by

J. P. Longwell and M. A. Weiss

Standard Oil Development Company
Esso Laboratories

(Manuscript submitted for publication March 1952)

TABLE OF CONTENTS

7. AIR-FUEL MIXTURE PREPARATION

by

J. P. Longwell and M. A. Weiss

INTRODUCTION

Liquid fuels for ramjet engines, once selected, metered and delivered to the injection points, must undergo several processes before combustion is possible. These processes begin at the injection point with atomization of the liquid, i.e., break-up of the liquid film or jet into small drops by the action of the injection device and/or the air stream. The drops must then be distributed throughout the air in proportions such that combustible mixtures exist in at least some local regions. During distribution, evaporation of the liquid also occurs.

The ultimate object of all of these processes is to obtain intimately (molecularly) mixed air and fuel in combustible proportions. This is the requirement to make burning possible and can be accomplished only when the fuel is in the vapor state, i.e., liquid drops cannot burn directly but first must evaporate.

For convenience, this section is divided into the three processes of atomization, distribution, and evaporation. None of these processes is understood well enough to permit precise design of practical combustors. However, there is enough information to obtain at least first approximations.

7.1 ATOMIZATION

Atomization consists of the breaking up of a large mass of liquid fuel into small drops. A complete analysis of this process would result in expressions describing the size distribution of the drops as a function of the fluid properties, system geometry, and operating conditions. Such an analysis is not available, although several mechanisms for atomization have been postulated.

The atomization process seems to be some combination of the following:

1. Spreading of the fuel jet into a cone, disk, or sheet by virtue of its own velocity,
2. Disruption of the liquid by virtue of its velocity relative to the air,
3. Breakage of thin sheets and ligaments into several drops by surface tension forces, and
4. Agglomeration of drops by collision.

The relative importance of each of these mechanisms depends on the details of the geometry, fluid properties, and fluid velocities.

The most successful qualitative explanations of atomization have come from high speed spray photography. Spark and/or flash pictures have been taken of various injection devices under various operating conditions. Figure 7.1-1 illustrates the behavior of a swirl-type atomizing nozzle discharging into still air. The fuel jet is rotating rapidly before leaving the nozzle orifice so that it spreads out into a conical sheet on discharge. The sheet becomes thinner as distance from the orifice increases. The effect of surface tension in breaking up the sheet is apparent from the

Fig. 7.1-1 SPRAY FROM A SWIRL-TYPE PRESSURE-ATOMIZING NOZZLE USING KEROSENE INJECTION AT TWO LB/IN^2

photograph; separated ligaments and sheets are formed which are drawn into drops. When drops formed under these conditions are collected, many are found containing entrapped air bubbles. It seems evident that the sheets of liquid fold over, causing the trapping. As liquid velocities increase, the conical sheet breaks up nearer the nozzle and finally appears to be torn apart as it comes into contact with the air. Few entrapped air bubbles are found under these conditions. It appears from photographs that the drops are then formed from ligaments or pieces short enough to form a single drop rather than breaking into several drops.

If fuel is introduced into the air stream through a tube at low-liquid velocity, it is found that when the air stream is of low velocity the liquid column is broken up (by surface tension forces) into drops with a diameter of the same order of magnitude as that of the column. As the velocity of the air increases, pieces are torn from the column surface and are stretched into thin ligaments which eventually break into drops. This mechanism is illustrated by Scheubel [1] in spark photographs at an air velocity of 80 ft/sec. With increasing air velocity, ligaments become less predominant (150 ft/sec) and the drops appear to form very near the column surface. The column itself is completely broken up a few tube diameters below the tube exit.

Some similar work was done at M.I.T.[2] in photographing streams of diesel oil injected (costream contrastream, and normal) into high-velocity air streams through five tubes of various radii. Semi-silhouette spark photographs were taken with an exposure time $< 0.25 \times 10^{-7}$ second at about room temperature and pressure. Nine typical pictures are presented in Fig. 7.1-2. Each part represents a constant fuel velocity at three different air velocities. The particular injection tube used here was about 0.11 inch outside diameter and 0.10 inch inside diameter. Sections (a) and (b) of Fig. 7.1-2 show costream fuel injection and Fig. 7.1-2(c) perpendicular injection. These photographs bear out the conclusions drawn from Scheubel's work. One additional feature, to be found in the perpendicular injection pictures, is the sweeping around of the fuel into the eddy zone directly downstream of the injection tube. This behavior tends to deposit fuel on the walls just below the tube and gives a markedly different distribution pattern from that obtained with a costream tube under otherwise identical operating conditions.

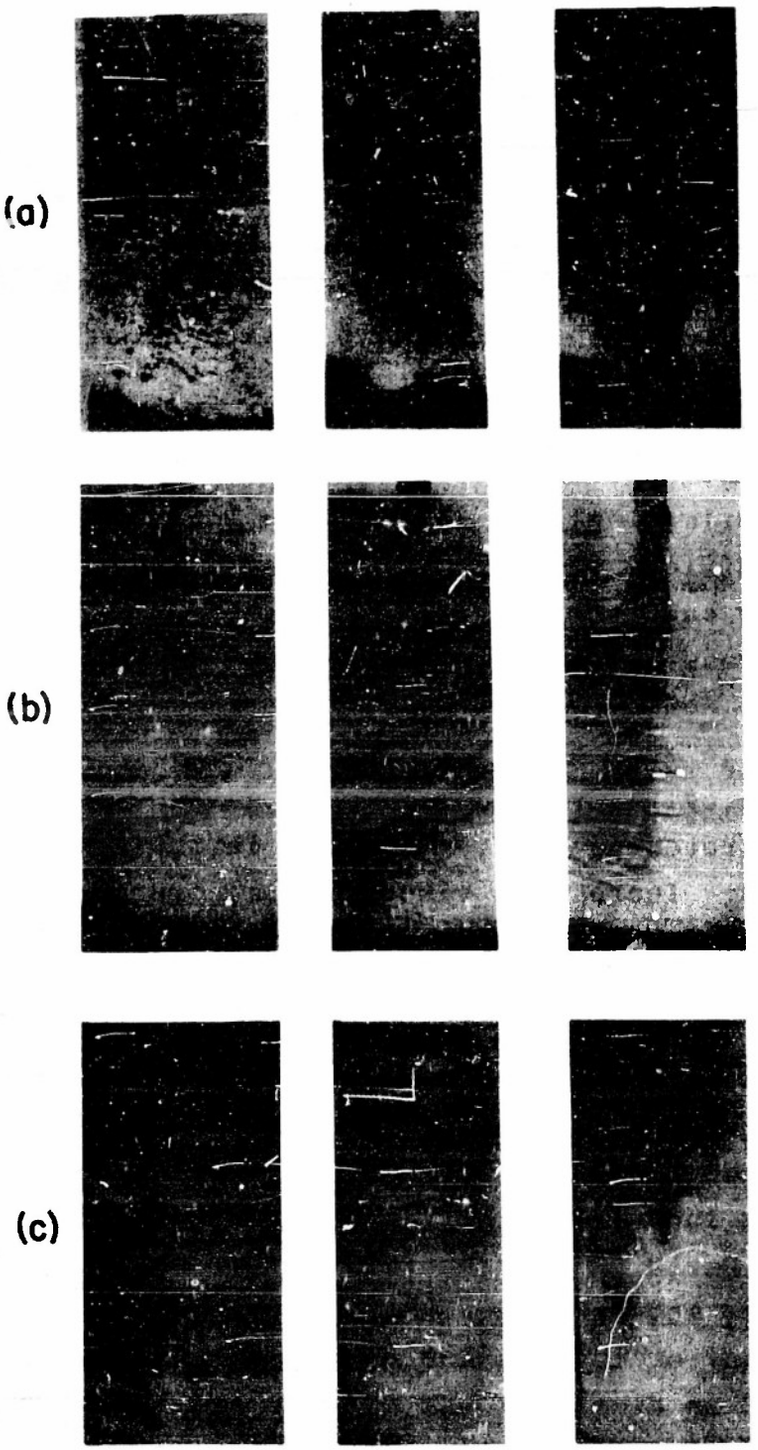

Fig. 7.1-2 INJECTION OF DIESEL OIL INTO A HIGH-VELOCITY AIR STREAM

(a) Costream injection; u_f = 3.5 ft/sec
(b) Costream injection; u_f = 1.2 ft/sec
(c) Normal injection; u_f = 1.1 ft/sec

The paragraphs above show the importance of relative velocity between the fluids. Other important factors which have been widely investigated are the physical properties of the fluids. Results of both theoretical and experimental work are available. Castelman [3], in discussing the formation of drops from ligaments, used Rayleigh's [4] calculation of the time of collapse of liquid cylinders. Taking surface tension and inertia forces into account, he found that the ligaments would collapse in a time of the same order of magnitude as that estimated from Scheubel's photographs.

A similar analysis was made by Weber [5] who considered, in addition, the effect of viscosity and density. From Weber's analysis, it is concluded that, as surface tension increases, a given ligament breaks up more quickly into drops. However, because the action of the air stream is probably to stretch the ligaments initially formed, thus reducing the cylinder diameter, high surface tension acts to reduce stretching time, resulting in the formation of larger drops. Increasing viscosity, according to Weber, increases the time for breakup of a given ligament, but it also results in larger drops being formed from that ligament. Furthermore, high surface tension and viscosity both tend to resist the deforming action of the air stream, probably resulting in larger ligaments being formed initially. Experiments have shown that an increase of either surface tension or viscosity increases drop size; confirmation is found in the work of David [6], Kuehn [7], Gelalles [8], Nukiyama and Tanasawa [9], and others.

A study of the breakup of single large water drops (0.5 to 5 mm in diameter) was made by Lane [10]. The drops were dropped in a steady-flow wind tunnel or were subjected to sudden blasts. At certain air velocities the drops were blown into the shape of a hollow bag which ultimately broke

up into smaller drops. However, the drops did not break below a certain critical velocity. For the steady-flow system at one atmosphere pressure this critical velocity could be expressed (in English units) as

$$(\Delta u)^2 d_o = 21.6, \qquad (7.1\text{-}1)$$

where Δu is the relative velocity between the drop and the air at the instant of breakage. Results for fluids other than water (the ratio of maximum to minimum surface tension was 17) showed that

$$\Delta u \sqrt{\frac{\sigma}{d_o}} \qquad (7.1\text{-}2)$$

The effect of viscosity in these experiments was minor except at very high viscosities (e.g. glycerol) in which cases breakup was retarded. If the equations above can be extrapolated to small drops, one would expect a 45 micron hydrocarbon drop to withstand relative velocities of about 200 ft/sec; small drops thus would be quite stable.

The preceding paragraphs have proposed a mechanism of drop breakup. However, the reverse of this process can also occur. Flow in the vicinity of the fuel-injection system of an engine is usually very turbulent. There is a certain probability that drops, once formed, will collide if their number per unit volume is large. On collision, two or more drops agglomerate into a single larger drop. This drop may not break again as its velocity relative to the air flow will probably be small. The distance between drops can be approximated from the volumes of air and fuel if the volume of air per drop is written as $\pi V_a d_o^3 / 6 V_f$. Assuming that the

drop volume is small relative to the air volume, and that the drops are arranged cubically, the distance between drops (in terms of drop diameters) is

$$s = \left(\frac{\pi V_a}{6V_f}\right)^{1/3} \qquad (7.1\text{-}3)$$

The distance between drops (measured in diameters) thus depends only on the volume ratio of air to fuel in the local region of interest. Nukiyama and Tanasawa [9] found that if this volume ratio was less than 5000 (corresponding to an s of about 14 drop diameters) an increase of average drop size was observed. Under practical operating conditions, s (calculated as above) may be less than 10 drop diameters so that collision and agglomeration are believed to be important factors.

Equations for Drop Size Distribution

A compact equation for reporting the distribution of drop sizes in a spray is desirable. Because there has been no successful theoretical analysis of the atomization process, various investigators have developed empirical formulae for this purpose. Several of these formulae are discussed in detail in [11] and [12]. The two most frequently used expressions are known as the Rosin-Rammler (R-R) and the Nukiyama-Tanasawa (N-T) equations. These are usually written in terms of Y (the fraction of material in the spray represented by drops with a diameter $>d_o$) or by the rate of change of Y with d_o.

$$\text{(R-R)} \qquad Y = e^{-0.693(d_o/\bar{d})^q} \qquad (7.1\text{-}4)$$

(N-T) $$Y = 1 - \frac{ad_o^q \left(\frac{6}{q}\right)}{\Gamma\left(\frac{6}{q}\right)} \qquad (7.1\text{-}5)$$

(R-R) $$\frac{dY}{dd_o} = \frac{-0.693q}{\bar{d}} \left(\frac{d_o}{\bar{d}}\right)^{q-1} e^{-0.693(d_o/\bar{d})^q} \qquad (7.1\text{-}6)$$

(N-T) $$\frac{dY}{dd_o} = \frac{qa^{6/q} d_o^5 e^{-ad_o^q}}{\Gamma\left(\frac{6}{q}\right)} \qquad (7.1\text{-}7)$$

In these equations Γ is the Gamma function, q is a distribution constant (high values of q give narrow drop size ranges), a is a size constant, and $\bar{d}$ the mass median diameter, i.e., the value of d_o at which Y = 0.5.

Other equations have been suggested in which y in the normal probability distribution curve is replaced by the logarithm of some function of d_o. One equation [12] of this type sets a maximum drop size--a more realistic assumption than the prediction of a few very large drops by other equations. Although these refinements give expressions which fit the experimental data more accurately, they are more difficult to handle mathematically. At present, the simpler equations appear adequate for conditions of practical interest. Bevans [11] has found that the Rosin-Rammler equation fitted the experimental data better for large drops than did the Nukiyama-Tanasawa equation. It is also more convenient to use when mass fractions are of interest. However, the Rosin-Rammler equation is not satisfactory when the number of drops is being considered because for $q < 3$ it predicts an infinite number of drops of zero radius.

Experimental Methods for Determining Drop Size Distribution

There have been very many experimental investigations of drop size distributions in sprays of various sorts. However, in only a few of these was the work extensive enough to permit general correlation of the results. Almost invariably a single injector or a single fluid has been used and only a single variable (if any variable at all) investigated. On examination of these data one finds that the lack of comprehensive programs has been the result of the extreme experimental difficulties encountered. The major effort in these programs has usually been directed toward development of a method for collecting and measuring the drops. As would be expected, this has resulted, not only in a paucity of data, but in a wide variety of collecting and measuring devices. It may be fairly stated that no method yet proposed is entirely satisfactory in all respects. The best procedures involve much tedious work. It is useful, therefore, to review the experimental techniques that have been developed. A long step forward in the understanding of atomization waits for a new, really satisfactory method of measuring drop size distributions.

The most common technique used for collecting and measuring drops involves coated slides. Such slides are placed in the spray path, exposed for a short time, and then immediately removed and photographed. Drops are counted and measured from impressions on, or in, the slide coating. Such counting and measuring are usually done microscopically or by projection of the photograph on a screen. Although the process is often manual, electronic scanning and counting devices have been developed, for example, by Rupe [13]. Such a device can obviously be used for classifying drops obtained by photographic image in any manner provided that the droplet images are sharp enough.

The slide coating is, of course, some substance in which the sprayed liquid is insoluble. There are two general types of coating in use. The first, usually magnesium oxide, is a soft thick deposit (thicker than the diameter of the largest drop). Droplets, on striking the surface, penetrate, leaving holes on the surface almost equal to the true droplet size. It has been found by May [14] that the observed hole sizes must be reduced by 15 per cent in order to give true droplet sizes. A second type of coating, usually soot or grease, is deposited on the slide in a very thin film. The drops, on striking, do not penetrate but flatten out to a certain degree. The amount of flattening (and thus the relation between the photographic impression and true drop size) must ordinarily be determined experimentally although Stoker [15] has proposed a correction equation.

Despite the fact that the slide technique is in common use, it suffers from several disadvantages. If the drop-size measurements are required in a moving stream, the physical size of the slide discriminates against collecting small drops (see Collection Efficiency) and measured average drop sizes will be too large. Furthermore, there is always the danger that drops will break on impact with the slide, or will evaporate either partially or completely before a photographic record is made, or that two or more drops will coalesce on the surface. Finally, in the absence of an electronic scanning device, there is the great tedium of measuring and counting enough drops to give a fair distribution.

A variation of this technique which, unfortunately, is useful only in static atmospheres, is the collection cell. Drops are permitted to fall from a spray into a shallow dish containing a liquid which is insoluble in the sprayed sample. Photographs are made of the dish and the droplets measured and counted. In one application of this method, Doble [16]

placed a photographic plate at the bottom of the dish and allowed the drops to sink through the liquid onto the plate surface. A parallel light exposure of the plate then gave true drop images directly.

The collection cell technique can be modified to a sedimentation method, again, useful only in static atmospheres. Giffen [17] placed a series of such cells at different distances from the nozzle. Observing that most of the drops in any cell were in a narrow-size range, depending on the cell distance, he was able to obtain distributions by measuring colorimetrically (using a dyed spray liquid) the volume caught in each cell. An initial calibration was required to correlate drop size with sedimentation distance.

The phenomenon of collection efficiency has been used for spray measurements in several different devices. In one type [18], an electrical charge is placed on moving droplets. The droplets then impinge on one of a bank of different sized cylinders and the cylinder charges measured. Collection by the cylinders will depend on the relation between drop mass and cylinder size and thus a rough classification may be made. In another type [19], drops are caught on magnesium oxide coated slides of various sizes. A classification of sizes on each slide is thus obtained.

The freezing technique in its several variations has shown promise for some applications. In essence, the drops are frozen either on or before collection and the distribution measured by sieving. The freezing process can take place in a gas (for example, by spraying molten paraffin wax into cold air), on a cold collecting surface, or in a cold liquid. Droplets (solidified) below about 60 microns must be measured by microscopy, sedimentation, or an elutriation technique. Several studies of this kind have been made [20,21]. The freezing technique allows accurate measurement of the resulting drops. However, the freezing process

must occur so as not to distort or break the drops before solidification or before the atomization process reaches equilibrium. This method may be useful for conditions of interest in ramjet application. For example, a molten wax of the same viscosity as the fuel to be used can be sprayed into a hot air stream. Freezing of the wax need not occur until the atomization process is complete (at some distance downstream) at which point the droplets can be solidified (by injection of cold gases) and readily counted and measured.

Various other approaches to spray measurement have been made which do not involve physical removal of the droplets in any form. One of the most familiar of these is that of Sauter [22]. The attenuation of a beam of light by a spray is measured photometrically to give a mean drop size. In this method, no information about the distribution can be obtained.

Direct photography of a portion of the moving spray would seem to be an obvious technique. However, it has not yet proved completely successful; the difficulties involved are noted by Fledderman and Hanson [23].

In still another device, a charged wire is placed in a spray stream and the voltage pulses caused by droplets impinging on the wire are counted and measured. This system is described by Geist, et al [24]. Although initially of great promise, the equipment has yet to show evidence of successful measurement of drops as small as would be encountered in average sprays.

Many other measuring devices have been proposed; the above paragraphs serve only as a brief (and incomplete) survey of the field. It should suffice to show the limitations of all present methods and the need for a new attack on the problem.

Collection Efficiency

Any object mounted in a flowing mixture of air and fuel drops will be selective as to the number and size of drops that strike the object. This selectivity is of obvious importance for the spray sampling devices mentioned above. It is also a factor in combustor development since the amount of liquid collecting on spark plugs, struts, flame holders, etc., may affect combustion. The selectivity arises in the following manner. Some distance upstream of the collector, the drops are presumed to be traveling in a straight line and with no velocity relative to the air. As the collector is approached (and potential flow around the collector is assumed) the streamlines curve, thus imparting a lateral drag force to the drops. If this drag force is large enough the drop will be deflected with the streamline and pass around the collector. If the drag force is not great enough, the drop is not deflected sufficiently but strikes the collector. Thus the phenomenon of collection efficiency occurs, depending on the relative values of drag and inertia forces. Collection efficiency is defined as the ratio of the number of drops striking the collector to the number of drops passing the upstream projected area of the collector. In general, collection efficiency increases as: (a) air velocity increases, (b) drop size increases, and (c) collector diameter decreases. There are lesser effects caused by other variables such as drop density, air viscosity, and collector shape.

Langmuir and Blodgett [25] have calculated these collection efficiencies as a function of the several variables and a few of their results have been rearranged and presented in Fig. 7.1-3. The parameter is a dimensionless group, Ω defined as $\Omega = \rho_\ell d_o / 9\rho_a d_c$ for the three collector shapes. The abscissa is the common logarithm of the drop Reynolds number,

defined as $Re = d_o u_a \rho_a / \mu_a$. From these curves, the influence of the several variables on collection efficiency should be clear.

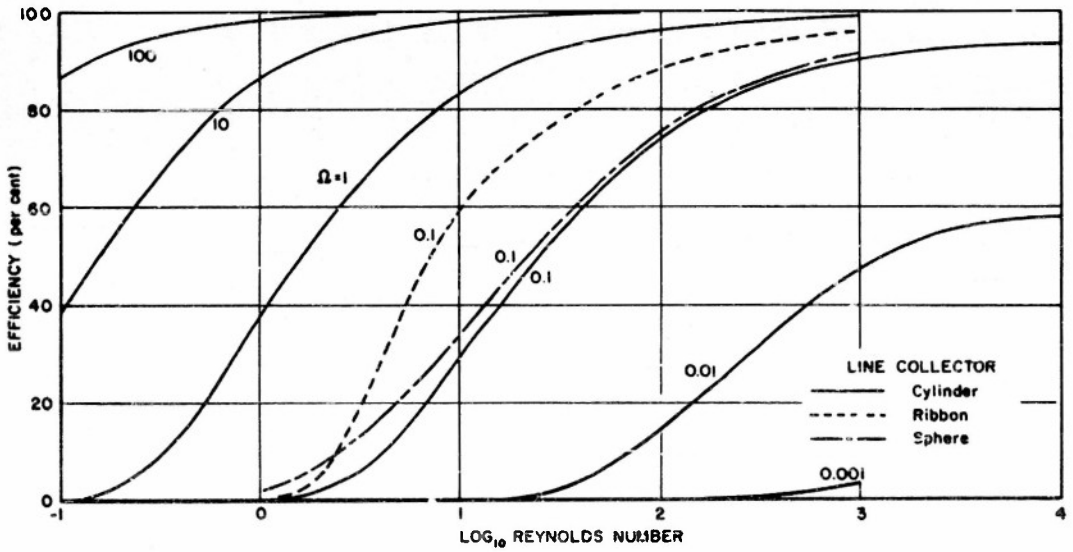

Fig. 7.1-3 COLLECTION EFFICIENCY OF VARIOUS SHAPES FOR SPHERICAL DROPS

Experimental Data--Air Atomization

Nukiyama and Tanasawa [9] have carried out an extensive series of measurements of the drop-size distributions obtained with a carburetor-type injector. Liquid (usually water) was injected through a small tube (0.2 to 2.0 mm) coaxial to a larger tube (2-5 mm) through which air was flowing in the same direction at velocities of 150 to 1000 ft/sec. A short distance downstream of the liquid tube exit, the mixture passed through a nozzle and into quiescent air. The spray samples, usually taken on the tube axis about 6 to 10 inches from the nozzle, were collected on glass slides coated with a viscous oil (when water was being injected). Exposure time of the

slide was about 1/300 second and at least 500 drops measured for each operating condition. The effects of exposure time and sampler location were studied and the data presented are believed to be representative.

Their results can be summarized by the following empirical formulae

$$2r_s = \frac{586\sqrt{\sigma_\ell}}{u_a\sqrt{S_\ell}} + 597\left(\frac{\mu_\ell}{\sqrt{\sigma_\ell S_\ell}}\right)^{0.45}\left(\frac{1000V_\ell}{V_a}\right)^{1.5} \qquad (7.1\text{-}8)$$

$$\frac{dY}{d(d_o/\bar{d})} = 286(d_o/\bar{d})^5\, e^{-5.7(d_o/\bar{d})} \qquad (7.1\text{-}9)$$

The units used, and the experimental ranges, are

$\bar{d}$, r_s - microns,

u_a - air velocity at nozzle exit (meters/sec),

V - volume discharge rate,

σ_ℓ - dynes/cm (19-73),

S_ℓ - specific gravity (0.7-1.2), and

μ_ℓ - centipoises (0.3-50).

For these data, the mass median drop diameter ($\bar{d}$) is 13 per cent greater than the surface to volume mean ($2r_s$).

Other variables, not accounted for in Eq. (7.1-8), were studied but their effects were usually minor. These included change of the nozzle to a sharp-edged orifice, variation of orifice and tube diameters, and movement of the nozzle relative to the liquid tube. It may be noted from Eq. (7.1-8) that, when the ratio of V_a/V_ℓ is less than about 5000, the

n becomes important, increasing drop size. This rdance with the comments on drop collision and agon previously made.

It may be assumed that the size of the slide-sampling device used was of the order of one centimeter. As discussed previously, this device has some bias against small (or low velocity) drops for which its collection efficiency is lower. At the higher air velocities used, it is estimated that the mean drop size reported is about 10 per cent too large because of this collection-efficiency effect. In addition, the actual distribution of sizes is not as narrow as reported. For lower air velocities drops were larger and the sampling error somewhat smaller. This source of error is not believed to be serious for most of the data.

In a ramjet engine, the fuel is usually injected into a large stream of high-velocity air. This is a different situation than that above in that air velocity is sustained after injection (instead of becoming quiescent). A good probability is that smaller drops would be obtained in such a system. Measurements made under such conditions would be of great interest.

Nukiyama and Tanasawa did not investigate the effect of air density or temperature; however, some work at the University of Illinois [26] shows that drop size increases with decreasing density or temperature. These variables need further examination.

As an example of the size drop predicted by Eq. (7.1-8), a mean drop size of 45 microns would result from the injection of kerosene into a 300 ft/sec air stream. This is much smaller than the drop size to be expected from a pressure atomizing nozzle operating in still air. Such operation commonly gives mean drop sizes of 100 to 200 microns.

Experimental Data--Pressure Atomizing Nozzles

A few detailed studies have been made [20,21,27] of atomization from swirl-type pressure nozzles. These results were obtained by discharging the nozzles into still air at room temperature. As such they are not representative of ramjet engine conditions under which a high-velocity hot-air stream usually impinges on the nozzle. However, the results are of interest at least directionally.

Longwell [21] examined the drops formed by atomizing nozzles by spraying hydrocarbon fuels, freezing part of the spray, and sieving. His results can be summarized by the empirical formulae

$$\bar{d} = \frac{R_i}{\sin\beta/2} \frac{0.72\, e^{0.007\,\mu_l/S_l}}{\Delta p_N^{0.37}} , \qquad (7.1\text{-}10)$$

$$Y = e^{-0.693(d_o/\bar{d})^q} , \text{ and} \qquad (7.1\text{-}11)$$

$$q = 1.35 + 0.45\left(\frac{\bar{d}}{100}\right) + 0.1\left(\frac{\bar{d}}{100}\right)^2 . \qquad (7.1\text{-}12)$$

The units used and the experimental ranges were

- $\bar{d}$ - microns (90-420),
- R_i - radius of nozzle orifice, microns (400-1400),
- β - spray cone angle (60-120 degrees),
- Δp_N - nozzle pressure drop, lb/in^2 (50-300), and
- μ - centipoises (10-100).

Viscosity has only a small effect at low viscosities, but, on reaching 13 centipoises, has increased drop size by

10 per cent. While some common fuels such as kerosene have low viscosities at room temperature, under some conditions they may be used cold enough to adversely affect atomization. Fuel sprayed into hot gases will heat as drops are formed, thus reducing viscosity. Spraying into a cold gas obviously reverses this effect. This is illustrated by tests in which two oils of the same injection viscosity (22 centipoises) were sprayed into air at room temperature. The first oil, injected at room temperature, gave a median drop size of 144 microns. The second oil, which was heated to 200°F to obtain its injection viscosity of 22 centipoises, gave a median drop size of 186 microns.

Several of the conclusions reached by Longwell are supported by the work of Giffen and Muraszew [17], who investigated pressure atomization of safety fuel. Drop sizes were measured either from impressions on magnesium oxide coated slides or colorimetrically by a sedimentation technique. It was found that mean diameters decreased as nozzle orifice size decreased, or nozzle pressure drop increased. A further conclusion was that centrifugal motion of the liquid leaving the nozzle helped atomization. However, the Rosin-Rammler equation did not represent the drop size distributions very successfully.

Schmidt [28] injected water through a hollow cone spray nozzle into a costream air flow (20 to 100 ft/sec). Measuring drops both photometrically and on magnesium oxide coated slides, he found that mean drop sizes decreased as nozzle pressure drop increased. There was also a trend toward smaller sizes as air velocity increased.

Molten paraffin was sprayed by Joyce [20] who collected and sieved the solidified drops. These data showed about the same dependence of drop size on pressure as found in Longwell's work; however, drop size depended on the orifice

diameter to the 0.6 power rather than a first power dependence as in Eq. (7.1-10). In the 75 micron range, Joyce obtained drop sizes about 60 per cent larger than Longwell did while results from larger nozzles (giving drops of 200-300 microns) agree well. The increase of the viscosity of paraffin while cooling in air may have interfered with atomization, thus increasing drop size.

7.2 MIXING AND DISTRIBUTION

Before combustion can occur, air and fuel molecules, in correct proportions, must be intimately mixed on a molecular scale. The final stage in this mixing process is accomplished by molecular diffusion. However, molecular diffusion is rapid enough to be practical over only short distances and fuel-injection points cannot be spaced as closely as these distances require. Therefore, when fuel is sprayed into an air stream, one must rely on the initial penetration and turbulent flow to provide most of the mixing, distributing the fuel well enough so that molecular diffusion can complete the final mixing stage.

The importance of quantitative knowledge of the mixing and distribution process is obvious in light of the effects of fuel distribution on combustor performance. In particular, this knowledge is required when operating at very lean mixtures. For this case, it may be necessary to restrict the distribution by limiting the amount of initially mixed air, so that combustible mixtures will be present and can be burned before the remainder of air is mixed.

A more detailed treatment of much of the material to follow can be found in [29]. This report considers at length experimental results, both in small-scale laboratory ducts and in full-scale combustors, together with the experimental techniques required to measure distributions. An extended derivation of most of the equations and calculation methods used here is also presented.

Turbulent Mixing

Diffusion resulting from turbulent velocity fluctuations occurs because small volumes of gas in turbulent flow

have a continuous random motion. This random motion is superimposed on the time average velocity of the stream. An average velocity of the random motion, $\sqrt{\overline{u^2}}$, is denoted as the turbulent intensity. In addition to intensity, another factor characterizing turbulence is the so-called scale of turbulence, ℓ, which is an average length of the random excursions. The scale is defined, using the variation of intensity with time, as

$$\ell = \int_{\theta}^{\theta+d\theta} \frac{u_\theta \, u_{\theta+d\theta}}{\sqrt{\overline{u_\theta^2}} \; \sqrt{\overline{u_{\theta+d\theta}^2}}} \, d\theta. \qquad (7.2\text{-}1)$$

The integrand of Eq. (7.2-1) is usually named a correlation coefficient.

According to the theory of turbulent diffusion, [30, 31], the rate of transport of material, w, is equal to a proportionality constant (E, the coefficient of eddy diffusivity) times the concentration gradient, or

$$\frac{\partial w}{\partial \theta} = - E \frac{\partial w}{\partial x} . \qquad (7.2\text{-}2)$$

Note the similarity between this equation and the equation for molecular diffusion. Although molecular diffusion is continuously occurring during the turbulent mixing process, the molecular diffusion coefficient, D, is usually less than 1 per cent of the eddy diffusion coefficient, E, and thus will be neglected here. The value of E is usually given by $E = \ell \sqrt{\overline{u^2}}$ and is proportional to the product of both scale and intensity of turbulence. Note again the analogy to D which is proportional to the molecular mean free path and the root mean square molecular velocity.

Equation (7.2-2) describes turbulent diffusion for a period during which a fairly large number of random motions occur. In a short time interval there are no changes in direction of motion of diffusing material. Therefore the proportionality constant E and the average distance traveled by diffusing material will depend chiefly on the intensity of turbulence and not on the scale. This latter case will often occur in ramjet application.

These considerations apply to the diffusion of material whose density is equal or comparable to that of the gas stream; the material thus has no difficulty in being transported along with the random gas motions. However, in the case of liquid droplets, the drop inertia interferes with the ability of the drops to follow the eddies, and the diffusion rate, through E, is reduced accordingly. A very rough estimation of this effect can be made by assuming that the velocity fluctuations in turbulent flow are sinusoidal and that Stokes law applies to the drag on the drop. The equation of motion of the drop is then

$$m \frac{d^2Z}{d\theta^2} = 3\pi\mu d_o \left(u_o \cos \omega\theta - \frac{dZ}{d\theta}\right), \qquad (7.2\text{-}3)$$

where Z is the drop displacement from its mean position, and u_o is the peak velocity of the air fluctuation relative to its time average velocity. Letting $\frac{3\pi\mu d_o}{m} = b$, a solution to Eq. (7.2-3) is

$$Z = \frac{bu_o}{\omega} \frac{b \sin \omega\theta - \omega \cos \omega\theta}{\omega^2 + b^2} . \qquad (7.2\text{-}4)$$

If Z_o is the maximum amplitude of gas motion relative to the mean position, $Z_o = u_o/\omega$ and therefore, dividing through Eq. (7.2-4)

$$\frac{Z}{Z_o} = \frac{b^2 \sin \omega\theta - b\omega \cos \omega\theta}{\omega^2 + b^2} \qquad (7.2\text{-}5)$$

The maximum value of Z, Z_m, can be determined by differentiating Eq. (7.2-5) and setting it equal to zero. If this is done,

$$\frac{Z_m}{Z_o} = \left(\frac{b^2}{\omega^2 + b^2}\right)^{1/2} , \qquad (7.2\text{-}6$$

where $\frac{Z_m}{Z_o}$ is the ratio of drop amplitude to gas amplitude. The frequency of motion of the drop is the same as that of the gas and therefore the velocity of the drop is reduced in proportion to the reduction in amplitude. Because the eddy-diffusion coefficient is proportional to the product of velocity and amplitude.

$$\frac{E}{E_o} = \left(\frac{Z_m}{Z_o}\right)^2 = \frac{b^2}{\omega^2 + b^2} , \qquad (7.2\text{-}7)$$

where $\frac{E}{E_o}$ is the ratio of diffusivity of the drop to that of a gas which could follow exactly the motion of the air stream.

To illustrate this effect, assume a 45 micron drop of kerosene in a 300 ft/sec air stream at atmospheric pressure. The frequency, ω, was estimated as 300 radians/sec for a 6-inch duct with fully developed pipe turbulence. For these conditions, $E/E_o = 0.35$. This reduction in diffusivity for

a drop relative to a vapor is of importance in engine design and is supported by experimental data cited later in this section.

Equation (7.2-2) may be solved in various ways to give time average fuel concentrations at any point. This information is useful for many purposes, but it should be kept in mind, throughout the discussion below, that no information is given as to instantaneous variation of fuel concentration. Information about variations with time would be required for precisely evaluating the mixing for combustion purposes. However, time average concentrations have been found to correlate well with combustor performance.

Flow conditions in jet engines are usually quite complex and there exists little knowledge about turbulence. This situation makes present use of turbulence theory difficult and direct measurement of diffusivity must be employed. However, knowledge of the effect of fuel distribution and mixing on combustor performance is not advanced enough to require greater accuracy in knowledge of the distribution itself than is presently attainable.

For application of Eq. (7.2-2), assume a duct large enough so that wall effects are negligible. Let an air stream flow through the duct with a velocity u which is constant at all points. If one assumes steady state, a constant E at all points, and negligible mixing in the flow direction (x) as compared to mixing perpendicular (r) to the flow direction, then by a material balance one obtains

$$\frac{\partial f}{\partial x} = \frac{E}{u}\left(\frac{1}{r}\frac{\partial f}{\partial r} + \frac{\partial^2 f}{\partial r^2}\right) \qquad (7.2\text{-}8)$$

expressed in cylindrical coordinates. Define f as the mass fuel to air ratio in any small volume of gas; it is more

convenient than, and a very good approximation to, a true concentration of fuel. Equation (7.2-8) may be integrated for a duct of infinite radius to give

$$f = \frac{W_f u}{4\pi W_a' E x} e^{\frac{-uR^2}{4Ex}} . \qquad (7.2\text{-}9)$$

Equation (7.2-9) is the "point-source" equation and describes fuel concentration downstream from a point source of fuel injection. Here, x is the distance of the survey point downstream from the source and R is the radial distance of the survey point from the axis of the source.

An experimental duplication of the conditions of the point-source equation can be carried out by injecting fuel at low velocity through a small tube in the center of a pipe through which air is flowing. Many such experiments have been carried out by various investigators. A sample of some data taken at the Esso Laboratories [29] is shown in Fig. 7.2-1. These results were obtained in 10-inch pipe with air flowing at 290 ft/sec at atmospheric pressure and 180°F. The average over-all fuel-air ratio was 0.01. Fuel/air ratios were measured at various radii at an axial station downstream and plotted as $\ln f$ against r^2. Such a plot, according to Eq. (7.2-9), should give a straight line with a slope equal to -u/4Ex. From this slope E can be calculated and thus eddy diffusivities are often determined by this type of experiment. It is interesting to note that the experimental data are very well represented by the line calculated from Eq. (7.2-9) despite the fact that, according to turbulence theory, E and u vary with radius. The presumption is that the ratio u/E remains constant.

According to measurements by Simmons [32], the scale of normal turbulence in the center of a pipe is approximately

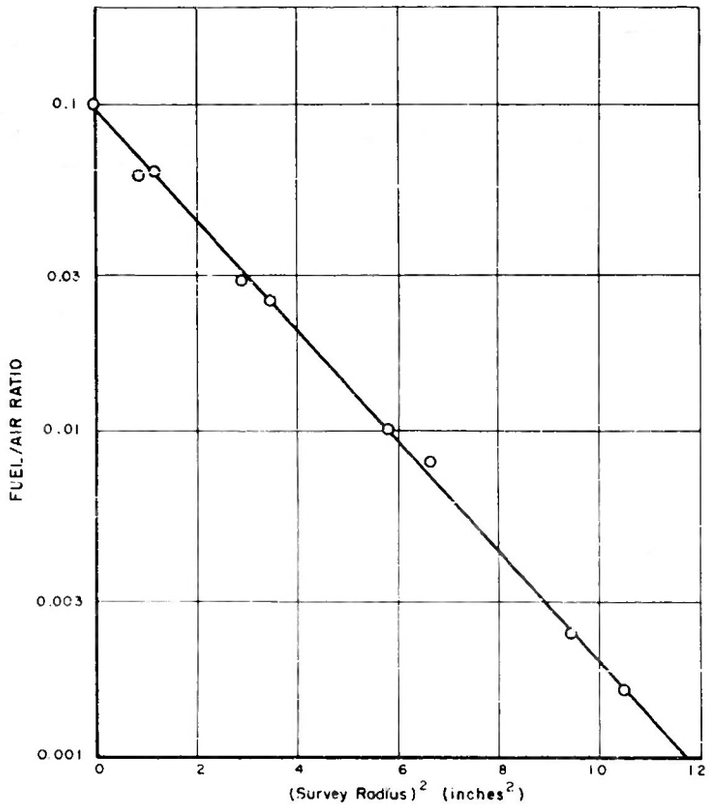

Fig. 7.2-1 DISTRIBUTION OF DIESEL OIL 34 INCHES DOWNSTREAM OF A POINT SOURCE

0.17 the pipe radius, and the intensity is approximately 3 per cent of the main stream velocity. The scale data suggest that diffusivity is proportional to duct diameter. Towle and Sherwood [33] found this to be true in their experiments on gaseous injection in long 6- and 12-inch ducts; diffusivity in the 12-inch duct was twice as large. The scale of turbulence is, however, very sensitive to duct length for short ducts and to the nature of flow preceding the section of interest. One cannot automatically assume

that changing the diameter of an engine combustion chamber will make a proportional change in diffusivity. Some experiments [29] in relatively short ducts have shown increases in diffusivity of only about 5 per cent in changing from a 6- to 10-inch duct. This result can be partly attributed to short-diffusion times during which, as mentioned before, intensity of turbulence is the dominant factor over scale.

If intensity is a constant fraction of average flow velocity, one would expect the ratio E/u of the point-source equation to be independent of velocity. Several investigators have shown that this is approximately true. In extensive work conducted at The University of Texas [34,35], for example, it was found that diffusivity increased linearly with air velocity. Such a result, of course, tends to keep the E/u ratio constant. In the Texas experiments, the changing apparent diffusivities unfortunately resulted not only from changing turbulent intensities but from a change in the behavior of the injection source (a disk-type nozzle) as well. This nozzle is a small disk, or ring, source whose effective radius changes with velocity. (Therefore the quantitative effect of air velocity on diffusivity cannot be readily estimated directly from these data.)

Furthermore, in the Reynolds number range encountered in jet engines (10^5 to 10^6), air density and temperature would not be expected to affect diffusivity greatly. This proved to be the case in experiments [29] in which a ten-fold variation in air density produced only minor changes in diffusivity. The conclusion is that E/u is primarily a function of geometry and that for a given geometry, according to Eq. (7.2-9), the fuel distribution pattern will be independent of operating conditions (assuming that the manner in which fuel is injected does not change).

These conclusions apply to a vaporized fuel, but, as shown by Eq. (7.2-7), the same rules do not apply to the diffusion of drops. Drop spreading also depends on drop size and turbulence frequency, the diffusivity ratio (E/E_o) decreasing with increasing size or frequency. Because of the frequency effect, E/E_o would be expected to decrease with increasing main-stream velocity. Quantitative prediction of this effect would require detailed knowledge of both atomization and turbulence. Neither is available. There are some data [29] for comparison of the diffusivity of a liquid spray (diesel oil, essentially unevaporated) and a substantially vaporized fuel, solvent naphtha. Both fuels were injected from a point source under identical conditions at various air velocities and atmospheric pressure. The results, in Fig. 7.2-2, show that the two diffusivities approach each other at low velocities, but that the diffusivity of diesel oil drops becomes much lower at high velocities. Some dropping off of the naphtha curve is also noted; the naphtha was not completely vaporized under test conditions. Atomization in these runs resulted from the impact of air on the fuel injected at low velocity through a constrastream tube.

For a vaporized fuel, a reasonable value of E/u is 0.001 foot for smooth flow in a 6-inch duct. However, for disturbed flow caused by the presence of miscellaneous struts, flame holders, etc., or other reasons, values of E/u up to 0.01 foot have been observed. For nonvaporized fuel, E/u should be decreased somewhat as illustrated in Fig. 7.2-2.

Equation (7.2-9) describes turbulent diffusion from a point source. If the fuel-injection device cannot be regarded as a point, the equation cannot be used directly. However, any nonpoint source can be pictured as an infinite number of point sources, properly arranged. The local fuel-air ratio at any point downstream will then consist of contributions from each of the infinite number of point sources

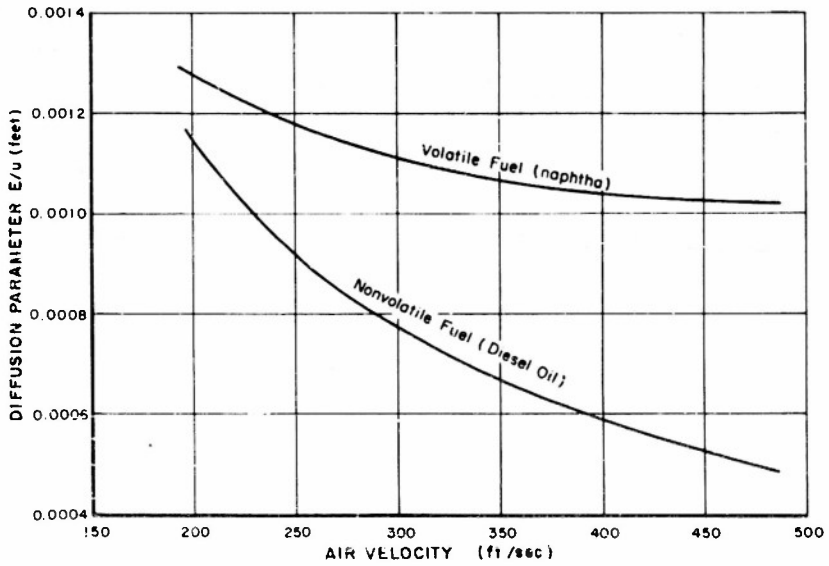

Fig. 7.2-2 EFFECT OF AIR VELOCITY ON THE DIFFUSION PARAMETER, E/u

making up the single nonpoint source. These contributions are calculated by assuming that each point source acts as though it were the only source present. It is easily shown that this is a mathematically rigorous procedure. Such calculations have been made for two such nonpoint sources that have been of interest, the ring (fuel issuing uniformly from the circumference of a circle) and the disk (fuel issuing uniformly from the entire area bounded by a circle). Their application will be discussed later. A similar technique may be applied to a finite source of any shape.

Summing up point sources around a ring of radius R_o, one obtains

$$f = \frac{W_f K}{W'_a R_o^2 \pi} I_o\left(\frac{2KR}{R_o}\right) \exp\left[-K(1 + R^2/R_o^2)\right] = \frac{W_f}{W'_a R_o^2}\ \phi, \quad (7.2\text{-}10)$$

where $K = uR_o^2/4Ex$, I_o is a modified Bessel function of zero order, and R is now the radial distance from the survey point to the ring axis. A detailed derivation for the ring source equation, and the disk source equation below, may be found in [36]. ϕ, a function of K and R/R_o, is plotted in Fig. 7.2-3 from the extensive tabulated data of Hardgrave and co-workers [37].

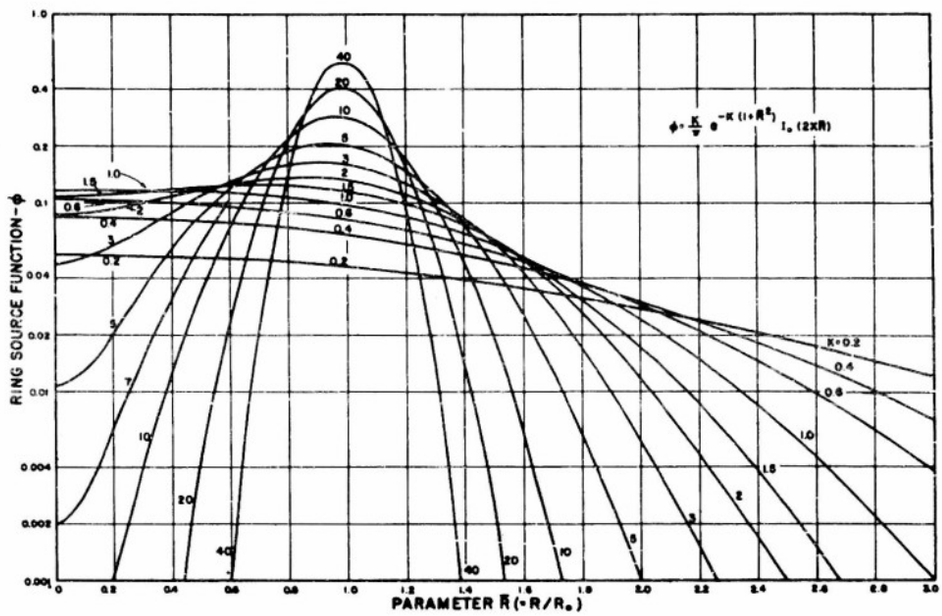

Fig. 7.2-3 THE RING SOURCE FUNCTION

This procedure may be carried another step by summing up ring sources over the entire area of a disk of radius M to obtain

$$f = \frac{W_f}{W_a' M^2} \frac{P}{\pi} e^{\frac{-PR^2}{2M^2}} \int_0^1 \frac{R_o}{M} e^{\frac{-PR_o^2}{2M^2}} I_o \left[P \frac{R}{M} \frac{R_o}{M} \right] d\left(\frac{R_o}{M}\right) = \frac{W_f}{W_a' M^2} \Psi , \tag{7.2-11}$$

where $P = uM^2/2Ex$. Ψ, a function of P and R/M is plotted in Fig. 7.2-4 from the tables of Kennedy [38].

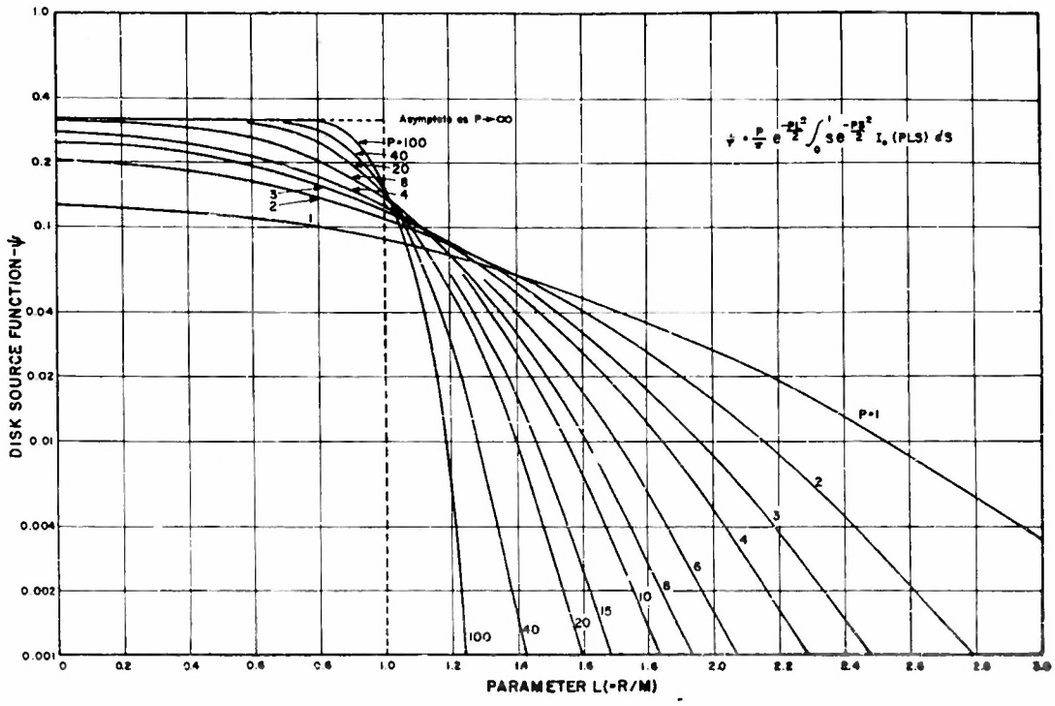

Fig. 7.2-4 THE DISK SOURCE FUNCTION

Each of the three equations, the point source (7.2-9), the ring source (7.2-10), and the disk source (7.2-11) has its specific application in ramjet design, depending on the type of injection device used. When fuel is injected into an air stream at low velocity through a small tube, it merely folds back over the end of the tube (for a contrastream tube) and passes downstream. A costream tube is even simpler. In either case the fuel source is effectively the end of the tube, a very small circle, and the point-source equation is applicable. However, when fuel is injected through a contra-stream tube at high velocity, the fuel jet penetrates the air stream. Before the fuel velocity can be stopped and reversed,

the jet has spread out radially, forming a cone (or frustum) whose apex is at the tube end and whose base is a circle which is now the effective source. A similar result is obtained with pressure atomizing nozzles for which the behavior is more obvious. In either case, the source is no longer a point but can now be regarded as a disk and the disk-source equation is thus applicable.

Use of the disk (or ring) source equation requires a disk (or ring) radius appropriate to the injection device and operating conditions. Many such radii have been determined for simple contrastream tubes and most of the results correlated in Fig. 7.2-5. The straight line shown is equivalent to the following equation.

$$\left(\frac{M}{R_i}\right) = 11.2 \left(\frac{\rho_a u_a^2}{\rho_f u_f^2}\right)^{-1/3} \qquad (7.2\text{-}12)$$

Note that both the ordinate and the abscissa are dimensionless. The ratio of effective disk radius to tube radius is a function of the ratio of momentum of air to fuel. These ratios were computed over a wide range of the individual variables, as shown in Fig. 7.2-5. Fuel velocities were calculated from the volumetric fuel flow rate assuming that the fuel filled the injection tube.

Effective disk radii were determined in two ways. In the first, the spray was photographed (or observed visually). The largest measured radius of the spray between the tube tip and a point 2 inches downstream of the tip was noted. This radius was then multiplied by 1.55 (an empirical factor) to give M. In the second method, an actual downstream distribution from the spray was obtained. Values of M were chosen by trial from the best-fitting disk-source equations. The two methods agreed quite well as can be seen from the data points of Fig. 7.2-5.

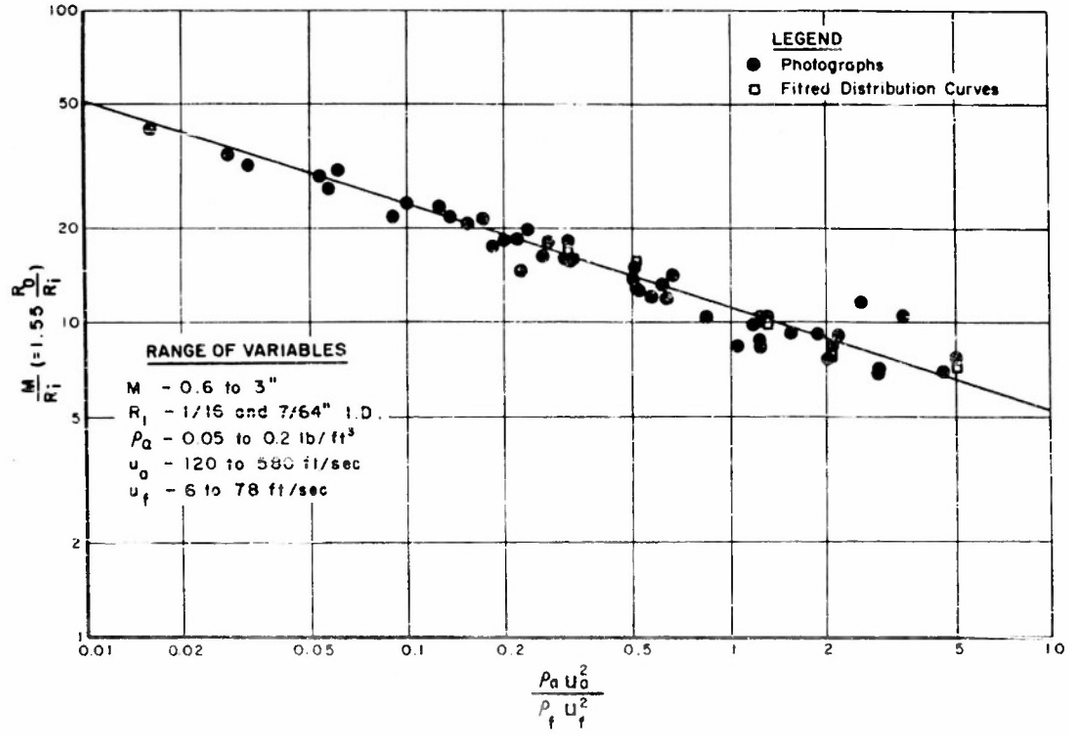

Fig. 7.2-5 CORRELATION OF INJECTOR RADIUS WITH OPERATING VARIABLES (CONTRASTREAM TUBES)

It is interesting to note that the observed spray radius (before multiplication by 1.55) is the radius to be used for the best-fitting ring-source equation. Ring-source equations were used to describe the distribution from these tube sources before tables of the disk-source equation became available. Although the ring source gives a fair approximation of the data, the disk source is usually more accurate.

Correlation of the proper disk radius for spray nozzles is more complex than for tubes. There are the additional complications created by nozzle body diameter, spray cone angle, and spray pattern. No general correlation is available at present and this represents a real failing in application

of the distribution equations to engine design. A few miscellaneous data were taken at atmospheric pressure with three nozzles whose orifice radii were 0.014, 0.032, and 0.047 inch. These nozzles gave hollow cone sprays with a semi-angle of about 40 degrees. At air velocities of about 250 ft/sec, the nozzles had effective disk radii (obtained by fitting distribution curves) of 3 to 4 inches when operated at 30 to 160 lb/in^2. The observed radii, multiplied by 1.55, ranged from about 2 to 2.5 inches. At an air velocity of 400 ft/sec, the 0.032-inch nozzle, operated at 50 lb/in^2, gave a disk radius of 2 inches, which agreed well with the observed value. Although these data are scant, they can be of value in determining the order of magnitude of spray radius to be expected.

One application of the disk-source equation is illustrated in Fig. 7.2-6. The data shown were taken for a pintle nozzle in a 10-inch duct at atmospheric pressure and an air velocity of 290 ft/sec. Diesel oil was injected at 0.2 lb/sec. Curves are shown representing the disk-source equation (M = 3.6 inches) and the point-source equation for the same diffusion coefficient (E = 0.35 ft^2/sec). Although the point-source equation completely fails to represent the data, excellent agreement is obtained by regarding the nozzle as a disk source. Initial spreading of the fuel is thus taken into account.

The importance of initial spreading caused by penetration of the fuel jet may be easily illustrated. Define a median radius, r_m, such that at any axial station half of the total fuel is distributed between r = 0 and r = r_m and the other half between r = r_m and r = ∞. From the point source equation one finds, in consistent units,

$$r_m = 1.66 \sqrt{\frac{Ex}{u}} .$$

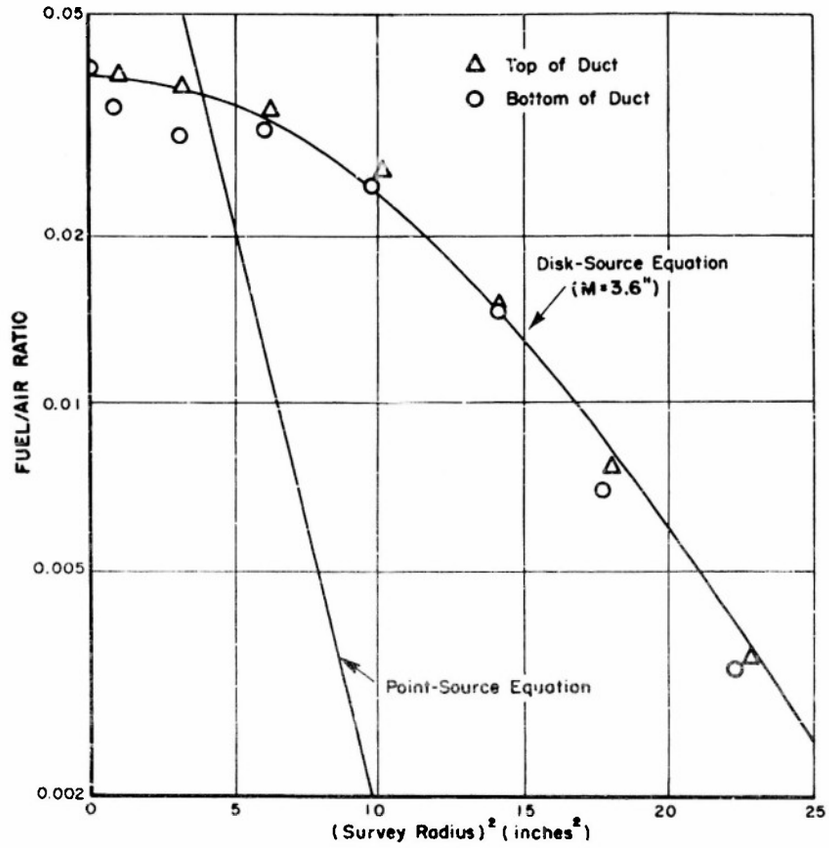

Fig. 7.2-6 DISTRIBUTION OF DIESEL OIL 35 INCHES DOWNSTREAM OF A SPRAY NOZZLE

If E/u is taken as 0.001 foot, the median radius (in inches) at various distances downstream is as follows:

x (feet)	0	1	2	3	4
r_m (point source)	0	0.63	0.89	1.09	1.26
r_m (nozzle)	2.25	2.31	2.38	2.45	2.52

The bottom row of the table gives values of r_m, for otherwise similar conditicns, when the injection source is a

typical atomizing nozzle. Note how much greater the spreading is, particularly in the first few feet, for the nozzle. One must travel 14 feet downstream from a point source to obtain the spreading found only one foot downstream from this nozzle. The figures above are for a vaporized fuel. For a nonvaporized fuel the difference would be even more marked because the initial penetration would be about the same but the diffusivity would be lower.

A common engine configuration for location of fuel-injection points is equidistant spacing around a large circle. For this type of injection geometry, the ring-source equation is useful. If a very large number of injection points on the circle is used, a true ring source is approached. For fewer points, the ring-source equation obviously gives progressively greater errors. Figure 7.2-7 may be used to find the distribution error in using the equation. For a given K and R/R_o, the parametric curves represent a given number of points on the circle required for an error not exceeding 10 per cent. The area below and to the left of each curve is a region of <10 per cent deviation. For example, for a K of 5 and an R/R_o of 1.0, the injection ring must have at least 8 points to give <10 per cent error. In these curves, R_o is the radius of the circle of points. W_f is the total fuel fed to all of the points.

Calculation of Fuel Distribution in Engines

Much development work on combustors involves adjustment of the fuel-injection system. Various injection devices are tri. and various radial and axial locations of the devices are used. It would be an obvious advantage to be able to predict the distributions resulting from these changes and thus eliminate at least part of the experimental work. This may be

done in many cases by use of the equations developed in the preceding section.

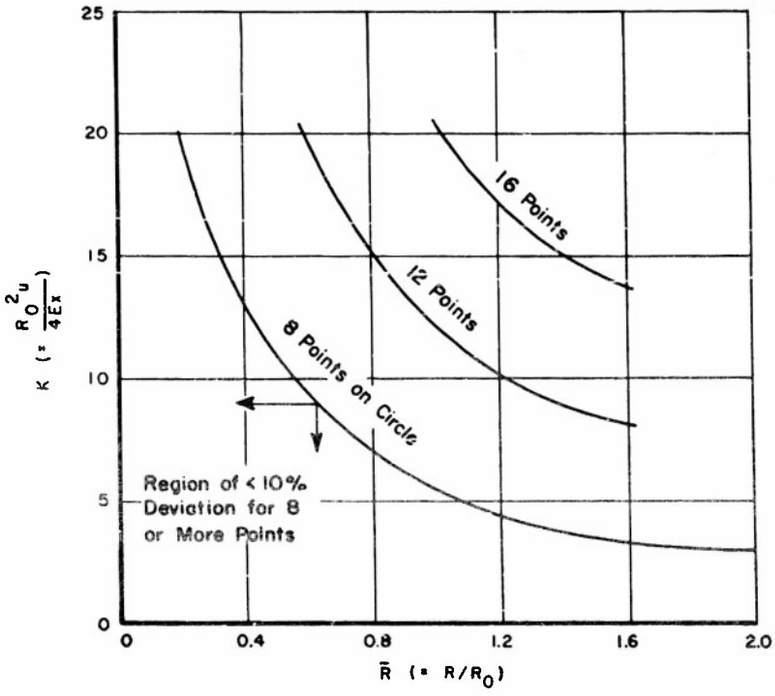

Fig. 7.2-7 CRITERIA FOR USE OF THE RING SOURCE EQUATION

Any practical engine configuration uses a number of fuel-injection points. The basis of the calculation method lies in the fact that at any downstream point, the total fuel present is the sum of contributions from each of the injection points if each of the points is considered as acting separately. The contribution from each point is represented by the point-source or disk-source equation, as is appropriate. For one or more circles of points, use of the ring-source equation will shorten the calculation procedure.

In general, the method is as follows. First, select the axial station at which the fuel distribution is desired. Next, select one or more radii in this cross-section. The number of radii necessary to survey depends, of course, on the degree of angular symmetry of the system. It is usual to choose at least two--one radius in line with as many injection points as possible and one radius midway between points. Along each radius, choose points about every inch from the duct center to several inches outside the outer wall. These outer points are required to correct for wall effects as will be discussed below. For each point on each radius, calculate the radial distance from that point to the axis of each of the injection points. Use Eq. (7.2-9) or (7.2-11) to obtain the contribution of fuel from each injection point. Sum up all of these contributions to obtain the total f at the radius point chosen. Repeat for all other radius points and for other radii.

This procedure is very tedious if done by analytical methods. A much simpler graphical method has been developed jointly by the Ordnance Aerophysics Laboratory and Esso [29]. This graphical method is restricted to the mild limitations that all of the injection devices be of the same type, are located at the same axial station, and are fed with equal amounts of fuel. If one or more of these requirements is not fulfilled, the graphical method may be modified accordingly and still represent a saving over the analytical method.

The first step here is preparation of a scale drawing of the cross-section at the injector station, locating each of the injector points. On this same drawing the survey radius (or radii) is chosen and plotted. Choosing Eq. (7.2-9) or (7.2-11), as appropriate to the injection devices used, a table is calculated of f as a function of R. All other variables in the equations are fixed by the geometry and operating

conditions. A transparent (plastic) rule is then made up, to the same scale as that used for the injector geometry, in which the divisions denote increments in R. However, for each R division the scale is marked with the corresponding f as determined from the prepared table. A pin hole is then located at R = 0. Such a rule is illustrated in Fig. 7.2-8.

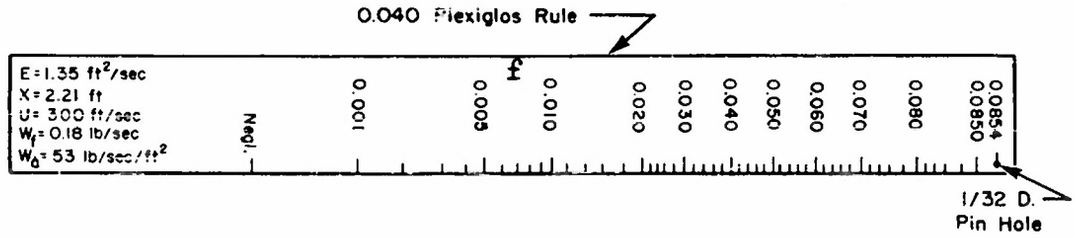

Fig. 7.2-8 PLASTIC SCALE FOR GRAPHICAL DETERMINATION OF FUEL DISTRIBUTION

A pin is placed, through the scale hole, at the radius point at which the fuel-air ratio is to be measured. The scale is then rotated about the pin and the reading for every injection point noted. These readings are tabulated and then summed to give the total fuel-air ratio. The process is repeated for other points and other radii. The results are usually plotted as a fuel-air ratio ordinate against the square of the survey point radius (relative to the duct axis). Reasons for using the square of the radius will be apparent in the discussion below.

Calculations up to this point have been subject to the limitations of infinite duct size (no wall effects) and constant air velocity (constant innerbody and outer wall diameters). These limitations may be removed by the following techniques.

When fuel, diffusing in a duct, reaches a wall, two results are possible. If the fuel is a vapor, it cannot collect or pass through and thus must diffuse back into the air stream. If the fuel is a liquid, it tends to collect on the wall and thus may be effectively removed from the system. This latter effect may be modified, as shown in recent work at the Massachusetts Institute of Technology, by reatomization. Droplets striking a wall on which a liquid film exists dislodge part of the film as other droplets which are picked up and carried by the air stream. For engine-design purposes, it is usually assumed that the fuel is vaporized, or, at least, will not be removed at the wall but will diffuse back. The technique of making graphical wall-effect corrections depends on the assumption that fuel diffuses from the wall as a mirror reflection (in r^2 coordinates) of the fuel which would have diffused beyond the wall if no wall were present. A rigorous solution for wall effects with a central point source has been developed [29]. However, the solution is complex, and much more complex for nonpoint and/or noncentral sources. The simple graphical techniques described below, though not rigorous, have proved entirely adequate in all applications to date.

An example of correction for outer-wall effect is shown in Fig. 7.2-9. The curve ABDE is calculated, using the transparent scale method above, ignoring the existence of the outer wall (at GDC). The area DGE is then rotated about GDC as an axis to give DGF. Each ordinate of the curve FD is added to the ordinate of curve ABDE with the same abscissa. The new curve, AGC, so obtained is the fuel distribution taking the outer-wall effect into consideration. It may be noted that these adjustments are performed on axes of f versus (duct radius)^2. On such a plot any area is proportional to a mass of fuel. In manipulating these curves, any areas which are transposed must be equal in order to preserve a material balance. For the example cited, note that area GDE = GDF = DCB.

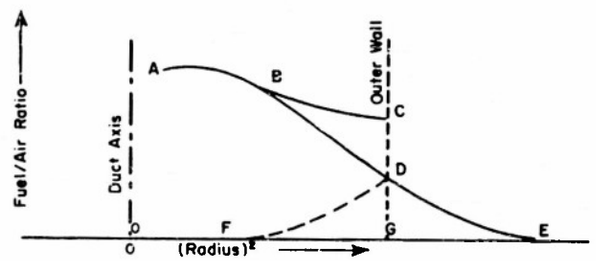

Fig. 7.2-9 CORRECTION FOR OUTER WALL EFFECT

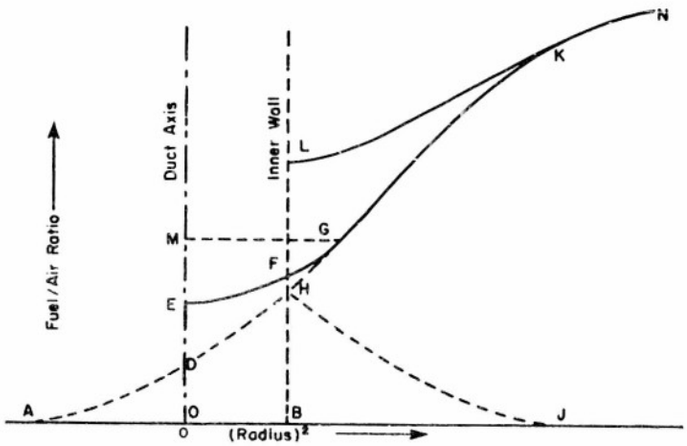

Fig. 7.2-10 CORRECTION FOR INNERBODY WALL EFFECT

Correction for innerbody effect is illustrated in Fig. 7.2-10. Basically the method is identical although somewhat more involved. Curve NKGFE represents the fuel distribution calculated as though no innerbody were present. Point D is located such that OD = DE. By trial and error a curve GHDA is drawn, tangent to NKGFE at G, such that MG = OA. Also, the vertical distances between AD and AO are equal to the vertical distances between EFG and DHG at any abscissa on the curves equidistant from the ODE (duct) axis. Curve HJ is formed by

rotation of HDA about the HB axis. Each ordinate of HJ is added to the ordinate (at the same abscissa) of HGKN to give LKN, the corrected fuel-distribution curve. It will be noted that a material balance is preserved because the deleted area EDOBHGF is equal to the added area KLFHG.

The second limitation to consider is that regarding changing innerbody and/or outer-wall diameters between the survey point and the injection station. A purely empirical correction is used that has proved satisfactory in practice.

The open duct area at the fuel-injection station is denoted as A_I, the area at the survey station as A_S, and the arithmetic average of A_S and A_I as A_A. In general A_S will be greater than A_I. A scale drawing of the injection-station cross-section and injector-point location is expanded by simple magnification of all radii so the original area A_I is made equal to A_A. In this process the injector-point locations will obviously also be altered. Using the graphical method above, calculate a fuel distribution (ignoring the existence of the walls) for this new injector geometry. In the disk-source and point-source equations all variables, except x, take on values corresponding to this new cross-sectional area A_A. x retains its original value, the axial distance from A_I to A_S. When the fuel-distribution curve is completed, multiply each value of the $(\text{radius})^2$ abscissa by A_S/A_A. This second curve approximates the fuel distribution at the survey station. Wall effects are then taken into account as described above.

Experimental Distribution Data for Full-Scale Engines

The calculation methods of the preceding section have been successful in predicting the results of not only idealized laboratory systems but of full-scale engines as well. Two

engines with baffle-type combustors were studied extensively--the RTV-N-6a, a ramjet 24 inches in diameter in the BUMBLEBEE Talos prototype program, and the XSSM-N-6, a Marquardt engine 28 inches in diameter designed for a Grumman missile. These two engines differed, for fuel-distribution purposes, in two important respects. First, the injection devices on the RTV-N-6a were low pressure drop tubes (point sources) whereas the XSSM-N-6 used pressure-atomizing nozzles (disk sources). Second, the air flow in the RTV-N-6a was quite disturbed whereas the XSSM-N-6 air flow was smooth.

As noted previously, an increase in flow disturbance will cause an increase in eddy diffusivity and thus an increase in fuel spreading. Therefore, diffusivities measured for smooth flow in laboratory ducts would not be expected to be applicable to the RTV-N-6a. The logical procedure would be to measure diffusivities in the engine directly. This was done for six different internal configurations each of which introduced a different degree of flow disturbance in the duct. The tests were made by injecting fuel at its usual rate through only one of the standard fuel tubes (located at its usual station) and measuring the distribution obtained at the flame-holder station (where all fuel surveys were made). Diffusivities were readily obtained, as pointed out in the discussion of the point-source equation, from the slope of the distribution curve. The results for the six configurations are plotted en masse in Fig. 7.2-11. Several points are of interest. First, the wide scattering of data indicates large variations of diffusivity with both duct radius and internal configuration (i.e., flow disturbance). Second, it was clearly shown that as configurations were tested which would be expected to progressively increase turbulence, average diffusivities across the duct similarly increased in accordance with the theory. Third, although diffusivity varied with radius, for a

given configuration, use of an average constant diffusivity in the calculations reproduced the later multi-injection point experimental data well within the required accuracy (20 per cent). Finally, laboratory data for the same conditions (300 ft/sec air flow at 300°F and 2 atmospheres pressure with naphtha fuel), but with smooth flow, predict an E of 0.6 ft^2/sec compared to average values in the RTV-N-6a ranging from 1.0 to 2.3 ft^2/sec, depending on the configuration used. All of these data emphasize the fact that in any engine with appreciably disturbed flow, eddy diffusivities must be determined experimentally for the specific configurations to be used.

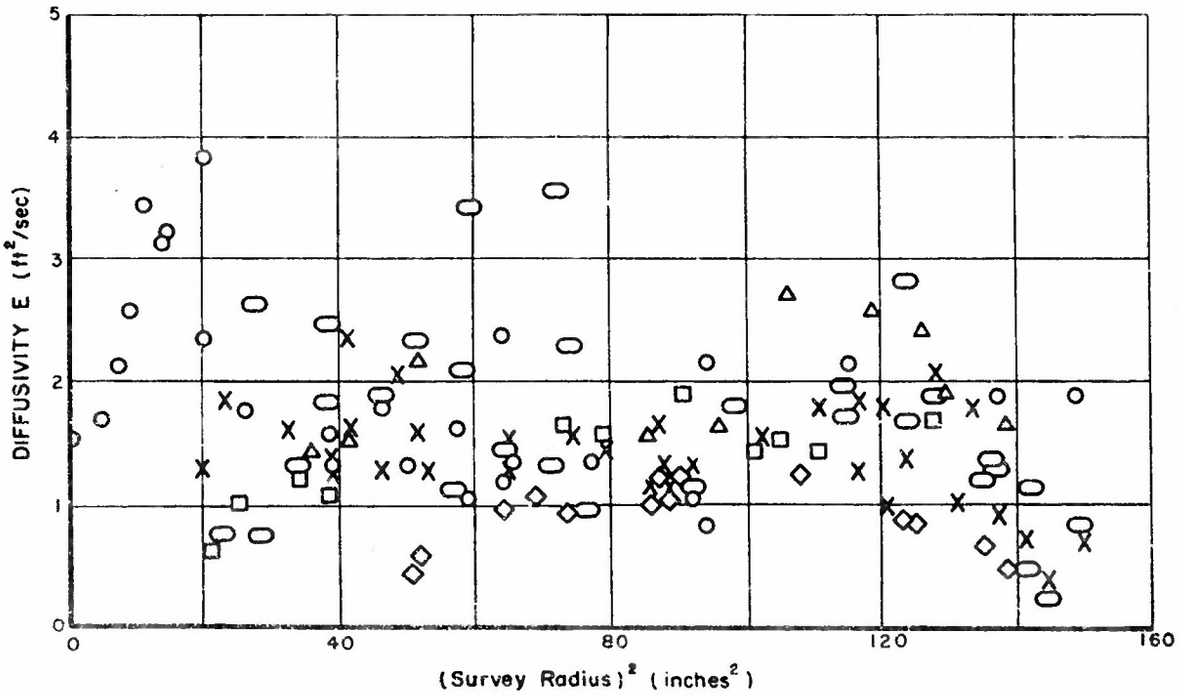

Fig. 7.2-11 DIFFUSIVITIES IN THE RTV-N-6a FOR SIX CONFIGURATIONS

After the RTV-N-6a diffusivities had been measured by these single-point injection tests, the various conventional multi-injection point fuel patterns were installed and the resulting fuel distributions observed. The four fuel patterns averaged about 50 injection points each. All patterns were symmetrical and any quadrant of each was laid out as illustrated (to scale) in the upper right corner of the sketches in Fig. 7.2-12. The small rectangles represent fuel spreaders fed by injection tubes shown as black dots in the rectangle centers. The "fuel spreaders" indicated consisted of short lengths of tubing split in half axially. These lengths were attached perpendicular to the upstream end of the injection tubes; the fuel issuing from the injection tube strikes the downstream center of the spreader and then flows equally to the two ends of the spreader before being exposed to the air stream. In this manner a spreader presumably converts a single injection tube into two point sources.

For comparison of the measured distribution curves with predicted ones, a diffusivity of 1.35 ft^2/sec (an average value for these configurations found in the single-injection point tests) was used. The graphical calculation method previously cited was used. Results for two different calculation techniques for each of the patterns are illustrated in the main sketches of Fig. 7.2-12 and are compared with the experimental data. The solid lines in Fig. 7.2-12 ignored the presence of the spreaders and simply considered each fuel-injection tube and spreader as a single point source. Th dotted lines were based on the assumption that the ends of the spreader acted as two individual point sources, each with half the total fuel flow to each tube. Behavior of the experimental data is something intermediate between these two cases although slightly favoring ignoring of the spreaders. In either case, the calculations predict the measured distribution well within

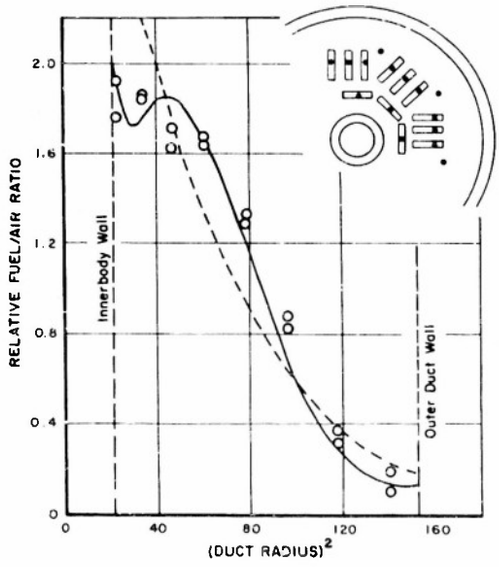

(a) Fuel Pattern 7116A

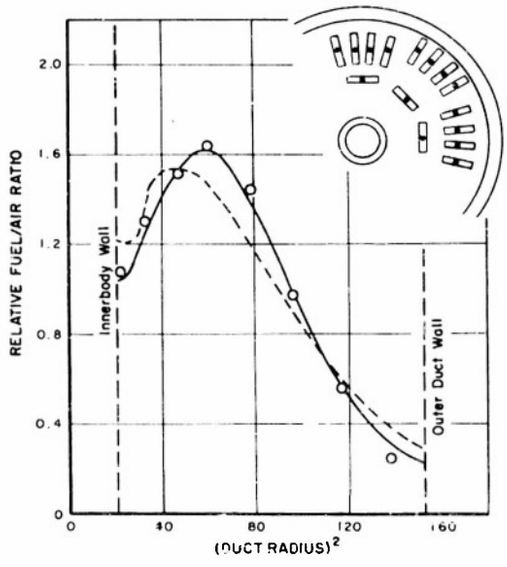

(b) Fuel Pattern 7427

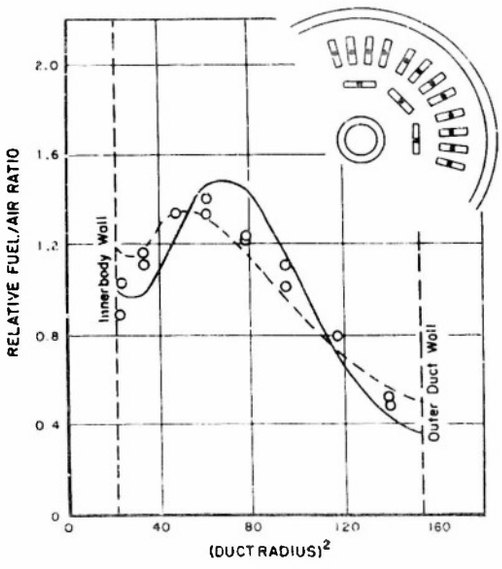

(c) Fuel Pattern 7337

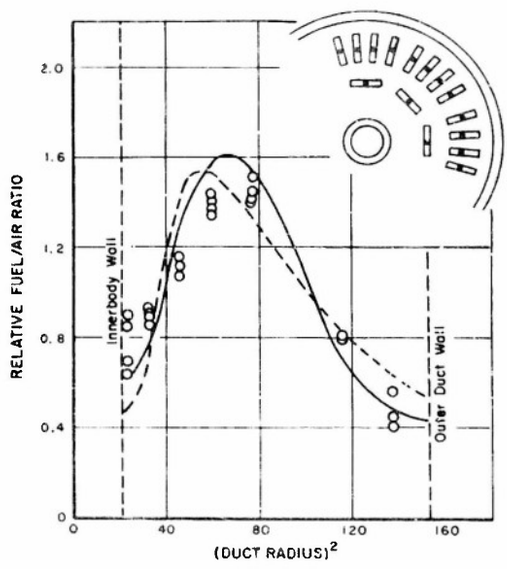

(d) Fuel Pattern 7338.5

Fig. 7.2-12 FUEL DISTRIBUTION IN THE RTV-N-6a

the accuracy deemed necessary (±20 per cent). Note, however, that deceptively small changes in the fuel-pattern geometry result in marked changes in distribution at the flame holder.

It is apparent that a converse situation exists in ramjet design. Rather than desiring the distribution from a given injector pattern, the distribution may be given and the necessary pattern desired. For a particular purpose, a homogeneous distribution was required in the RTV-N-6a. Such a distribution obviously required spacing of the injector points equidistant from each other at the intersections on an equilateral triangular grid. The closeness of spacing depends on the degree of homogeneity required. In this case the pattern was designed so that the survey f on the axis of an injection point would be within 3 per cent of the survey f on an axis midway between injection points. The spacing was computed, by trial and error, to be 2.75 inches. Several additional points were added near the walls for homogeneity in that area. Such an injection pattern was constructed and tested with the results shown in Fig. 7.2-13. The design distribution was achieved well within the accuracy required. Although a homogeneous distribution is a relatively simple one, similar techniques may be used for the drawing board location of injection points for any type of distribution.

Testing in the XSSM-N-6 was somewhat simpler than in the RTV-N-6a. Only two fuel patterns were used, each consisting of 24 contrastream high-pressure hollow-cone spray nozzles equally spaced on a circle located 30 inches upstream of the flame holder. The patterns differed only in circle diameter, 22 inches and 24 inches. Because of the smooth flow, diffusivities were assumed to be equal to those observed in laboratory tests (E/u = 0.0020 ft) for similar operating conditions. Fuel-distribution surveys were taken in two quadrants.

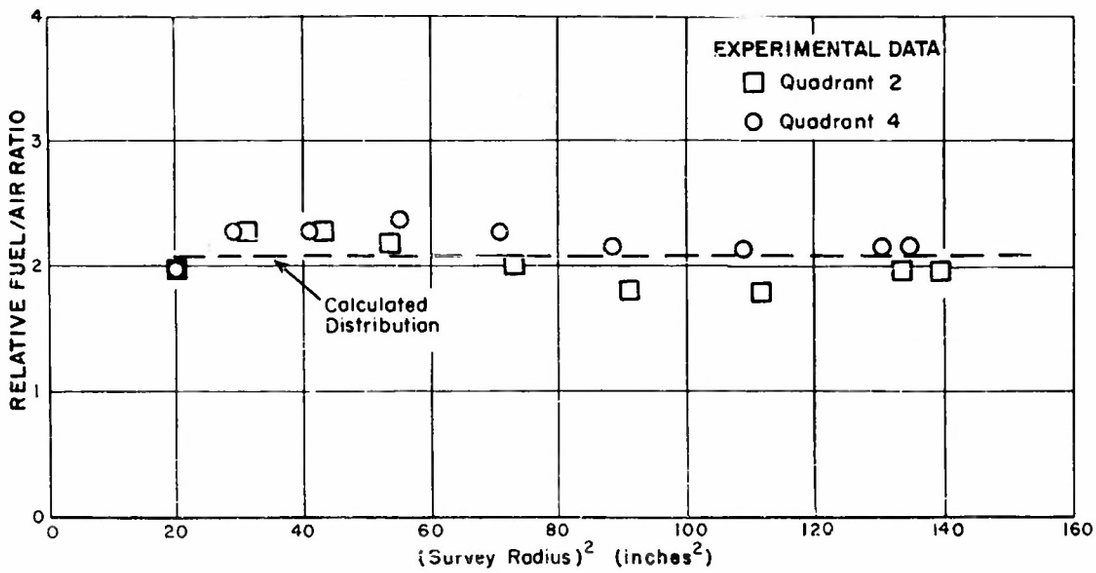

Fig. 7.2-13 HOMOGENEOUS DISTRIBUTION IN THE RTV-N-6a

In Figs. 7.2-14 and 7.2-15 the experimental data are presented for the 22-inch and 24-inch nozzle circles respectively. Three calculated curves are shown on each figure. They differ as follows:

1. The dotted curve was calculated assuming each nozzle to be a separate small ring source. (Note: Ordinarily the disk-source equations are used for nozzles. However, at the time of these tests, tabulated values of the disk-source equation were not available. Small ring sources are fair approximations to nozzle behavior. Had the disk-source tables been available, the calculated curves would represent the experimental data more closely than the present dotted curves.) The predicted value of E/u (0.0020 ft) was used.

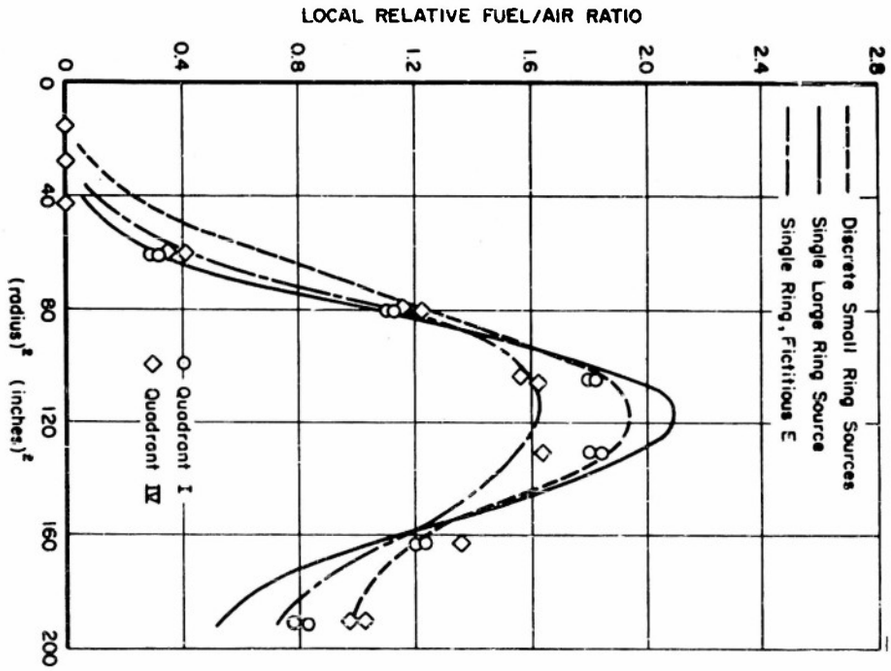

Fig. 7.2-15 FUEL DISTRIBUTION IN THE XSSM-N-6
Nozzles were on a 24-inch-diameter circle

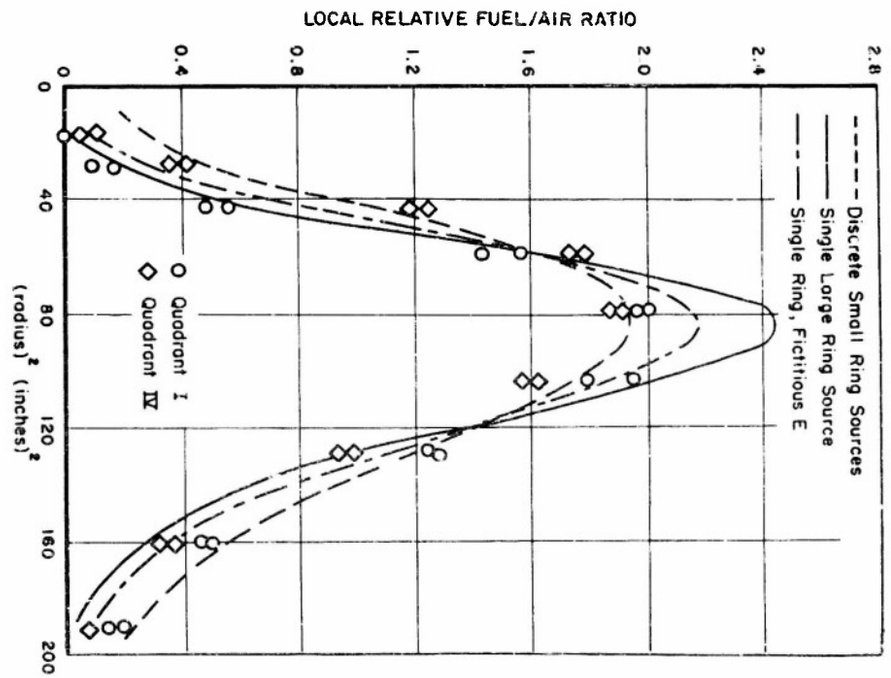

Fig. 7.2-14 FUEL DISTRIBUTION IN THE XSSM-N-6
Nozzles were on a 22-inch-diameter circle

2. The solid curve was calculated assuming the circle of nozzles to be a single large ring source with a radius of 11 inches or 12 inches as appropriate. Again, E/u was 0.0020 ft.
3. The dot-dash curve was calculated as in 2 above but an E/u of 0.0026 ft was used. This value was found, by trial, to best fit the data. E was thus increased from 0.45 to 0.57 ft^2/sec, an increase expected in order to account for the initial spreading caused by the nozzles. This spreading is not accounted for in the ring-source equation using the predicted diffusivity.

Comparison of the calculated curves with the experimental data shows better agreement, using the predicted diffusivity, of the curve calculated from 24 discrete nozzle sources than the single-ring source curve. The third plot, using a higher diffusivity and a single-ring source, is slightly better than the other two. The conclusions to be drawn are that the circle of nozzles actually behaves more like discrete sources than a single ring. If the single ring is used, to cut down calculating time, the diffusivity must be increased to account for initial spreading. This increase must be determined from past experience or by trial fitting of the best ring-source curve to a few sets of multi-disk source curves.

The object of the foregoing sections has been to demonstrate that calculation of fuel distribution in full-scale engines is not a hopeless task. For many engines it can be done well within the accuracy required for design purposes. Measurement of diffusivity by single-point injection, if necessary, is relatively simple and in any case is much simpler than cut-and-try experimental methods of manipulating the fuel-injection geometry. It is hoped that this work, which is only an introduction to the field, will stimulate wider interest in the

possibilities of predicting fuel distributions in ramjet engines. The demonstrated effects of fuel distribution on combustor performance (see Chapters 9 and 10) can make such interest a profitable one.

7.3 EVAPORATION OF FUEL DROPS

The mechanism and rate of combustion depend on whether or not the fuel is vaporized. It is therefore of interest to determine the extent to which fuel, injected into an engine air stream, will evaporate. The limiting degree of vaporization that can take place is the equilibrium vaporization, a function of the fuel volatility, the relative amounts of fuel and air present, temperature, and pressure. Equilibrium vaporization is defined as the fraction of fuel that will have been vaporized after infinite time (i.e., at equilibrium) if given quantities of fuel and air are mixed in an isolated system at a given temperature and pressure. In general there is not sufficient time available for equilibrium vaporization to occur so that equilibrium represents only a limiting condition. In this usual case it is profitable to examine the factors contributing to the rate of evaporation in order to determine what fraction of the fuel, necessarily lower than the equilibrium fraction, will vaporize.

Equilibrium Vaporization

Calculation of the equilibrium vaporization in air of any multi-component fuel is a special case of the general vapor-liquid equilibria relationships. Such a calculation can always be performed by means of material and energy balances and the appropriate equilibrium equations. Consider a fuel of n components in which i is any particular component. By an energy balance, in an adiabatic process,

$$w_f H_{f_i} + w_a H_{a_1} = \sum_{i=1}^{n} w_{l_i} H_{l_i} + \sum_{i=1}^{n} w_{v_i} H_{v_i} + w_a H_{a_2} . \quad (7.3\text{-}1)$$

In this equation the molar enthalpies (H) are functions of temperature only. To the energy balance may be added the material balances,

$$w = \sum_{i=1}^{n} (w_{\ell_i} + w_{v_i}) \quad \text{and} \quad w_i = w_{\ell_i} + w_{v_i}. \quad (7.3\text{-}2)$$

Finally, the equilibrium equation is

$$p_i = C_{E_i} \frac{w_{\ell_i}}{\sum_{i=1}^{n} w_{\ell_i}} \quad \text{and} \quad \sum_{i=1}^{n} p_i + p_a = p. \quad (7.3\text{-}3)$$

In general C_{E_i}, the distribution coefficient, is a function of composition, temperature, and pressure and is obtained from the literature [39,40]. The equations above are usually solved by trial, assuming a certain temperature and adjusting the fraction vaporized until all of the equations are satisfied. This procedure may always be used but is very tedious when the fuel consists of more than two or three components. In the case of hydrocarbon fuels, a very large number of components is present and a component breakdown is not ordinarily available. The distillation data for such fuels may be used in the method above by arbitrarily dividing the fuel into several portions, each with a narrow boiling range. These portions are then treated as pure components using appropriate average physical properties. Such properties have been compiled conveniently by Maxwell [40] from whose book part of the empirical method of the appendix has also been taken. Use of the empirical method just cited is recommended for any fuel consisting of more than two or three pure components. This method is explained in detail in the appendix and a sample calculation given.

Using the empirical technique, equilibrium vaporizations of AN-F-32 and No. 1 solvent naphtha have been calculated for various operating conditions. The data, in Tables 7.3-1 and 7.3-2, give air temperatures (^{o}F) before mixing for specific pressures, air-fuel ratios, and fractions of fuel vaporized. Inlet fuel temperature was assumed as 80^{o}F.

It is of interest to note that for most of the common conditions of engine operation, the fuel can completely vaporize despite the fact that the air temperature before mixing is considerably below the average boiling point of the fuel. Since incomplete vaporization is frequently observed at the flame holder, this illustrates the fact that although equilibrium vaporization is the limiting condition, it is often not achieved. For a given geometry and operating condition, the cure is better atomization and distribution. From the tables, a rough idea of the air temperatures required for complete evaporation may be estimated. For stoichiometric quantities of AN-F-32 (with a boiling point of about 385^{o}F at the 50 per cent point on an ASTM distillation curve), 100 per cent vaporization is possible if the entering air is as much as 125^{o}F below this 50 per cent point. The above figure is for a static pressure of one atmosphere. For other pressures, this figure varies (after converting the 50 per cent point to equivalent temperatures at the other pressures) from 65^{o}F (at 0.1 atmosphere) to 185^{o}F (at 4 atmospheres) below the converted 50 per cent point. Similar values calculated for solvent naphtha (normal 50 per cent point of about 185^{o}F) average about 20^{o}F below the figures cited above.

Data of the type in Tables 7.3-1 and 7.3-2 have proved useful in investigating the variation of equilibrium vaporization with altitude in a climbing ramjet missile. Increasing

temperature increases, and increasing pressure decreases vaporization. This explains the fact that vaporization is poorest at intermediate altitudes. That is, starting from sea level, temperature decreases at an effectively faster rate than pressure, making equilibrium vaporization poorer. However, on reaching the stratosphere, temperature remains constant while pressure continues to decrease so that vaporization again increases. All of the above assumes a reasonably constant Mach number. At Mach numbers of 1.6 to 2, for example, using stoichiometric ratios of air to AN-F-32 fuel, the poorest vaporization occurs at an altitude of about 35,000 feet for average atmospheric conditions.

TABLE 7.3-1

Calculated Equilibrium Vaporization of AN-F-32

Air Temperatures Before Mixing - °F

Air Fuel Ratio	S/1	10/1					15.1/1					22/1					30/1				
Pressure - Atm Abs	4.0	0.1	0.5	1.0	2.0	4.0	0.1	0.5	1.0	3.0	4.0	0.1	0.5	1.0	3.0	4.0	0.1	0.5	1.0	2.0	4.0
10% Vaporized	181	38	85	106	130	156	51	70	88	110	133	94	96	78	96	118	18	81	68	87	106
30 "	382	85	116	172	200	228	77	123	148	171	198	96	106	127	150	174	58	96	118	137	160
50 "	338	132	186	213	240	275	109	167	160	207	234	91	136	157	183	208	81	133	144	136	191
65 "	372	184	310	337	386	386	128	177	202	229	256	108	153	178	201	226	96	138	160	183	209
78 "	386	171	237	366	386	317	140	190	216	348	873	118	163	186	213	239	108	148	170	196	220
88 "	433	190	246	274	304	337	157	207	333	381	881	133	179	309	48	896	118	188	188	308	838
100 "	464	323	278	307	338	371	184	234	881	386	318	168	205	830	856	283	143	187	310	234	260

TABLE 7.3-2

Calculated Equilibrium Vaporization of No. 1 Solvent Naphtha

Air Temperatures Before Mixing - °F

Air Fuel Ratio	S/1	10/1					15.1/1					22/1					30/1				
Pressure - Atm Abs	4.0	0.1	0.5	1.0	8.0	4.0	0.1	0.5	1.0	3.0	4.0	0.1	0.5	1.0	8.0	4.0	0.1	0.5	1.0	2.0	4.0
10% Vaporized	-18		-90	-73	-83	-30		-96	-78	-88	-38			-81	-69	-48			-85	-71	-53
30 "	78	-73	-34	-12	13	88		-43	-38	-3	30		-82	-34	-14	8		-88	-43	-26	-8
50 "	127	-50	8	29	84	83	-80	-11	9	38	84		-24	-8	15	36		-33	-18	4	24
65 "	196	-18	31	84	81	110	-32	8	31	84	78		7	12	38	58		-18	-1	20	42
78 "	196	8	48	71	96	127	-18	21	44	70	83	-33	4	24	48	88		-8	10	21	53
88 "	207	18	96	88	118	143	-8	24	58	83	107	-12	18	38	59	84		9	28	41	66
100 "	286	50	96	181	149	177	21	96	88	113	138	3	41	81	83	108	-11	36	44	66	90

Evaporation Rate of a Single Drop

Equilibrium conditions are not often attained in a ramjet engine. Therefore the rate at which evaporation occurs, and thus the closeness with which equilibrium is approached, becomes of interest. Calculation of evaporation rates is much more complex than calculation of equilibrium vaporization. In most cases, the absence of necessary physical data precludes anything but very rough approximation. In the section that follows, no attempt will be made to give a design procedure for evaporation similar to that for distribution. The purpose of this section is to offer only a general survey of the problem. Major factors affecting evaporation rate will be pointed out and an attempt made to indicate the order of magnitude of their effects. The conclusions reached can be summarized briefly here. Increase of evaporation rate can be accomplished in several obvious ways, through increase of fuel volatility and/or increase of fuel temperatures. Less obvious is the fact that increased air velocities and turbulent intensities will also increase the degree of evaporation at any given station. Finally, the great importance of good atomization is realized, one of the few variables in which the designer has much latitude to work.

These factors may now be examined in detail. Although a practical evaporation problem will be very complex, it is profitable first to set up a simple system and then examine the effects of the simplifying assumptions.

Assume that a single pure liquid drop of constant radius exists in air, that there is no relative velocity between the drop and the air, and that steady state prevails. These assumptions imply that concentration and temperature gradients around the drop adjust rapidly compared to their rate of change with time as the drop evaporates. In these circumstances the

rate of evaporation depends on the rate at which heat is transferred to the drop, this heat supplying the latent heat of vaporization. The evaporated material formed must then diffuse away from the drop surface. This diffusion rate depends on the partial pressure of fuel at the surface and thus on the drop temperature. A further assumption is that the vapors immediately surrounding the drop are in equilibrium with the liquid. From these considerations it is clear that the drop attains an equilibrium temperature below the boiling point, depending on the relative rates of heat and mass transfer.

If spherical symmetry is assumed (all physical properties are functions of distance from the drop center only) the following equation for heat transfer may be written

$$\frac{\partial Q}{\partial \theta} = - kA \frac{\partial t}{\partial r} + m_o c_p t. \qquad (7.3\text{-}4)$$

The first term on the right is the familiar one for heat conduction. The second term accounts for the sensible heat carried by the diffusing vapors; a consideration of importance at high evaporation rates. A heat balance across a differential change in r for steady state gives

$$\frac{m_o}{4\pi} \frac{d(c_p t)}{dr} = r^2 \frac{d(k \frac{dt}{dr})}{dr} + 2rk \frac{dt}{dr} .$$

While k and c_p change with temperature, it is assumed that they are constant at appropriate average values, and thus integrating:

$$\frac{t_1 - t}{t_1 - t_o} = \frac{\exp \gamma r_o/r_1 - \exp \gamma r_o/r}{\exp \gamma r_o/r_1 - \exp \gamma} , \qquad (7.3\text{-}5)$$

where $\gamma = -m_o c_p / 4\pi k r_o$ and r_1 is the radius at which bulk air stream conditions are assumed to exist. The heat entering the drop surface supplies latent heat only and thus one can write

$$\lambda m_o = 4\pi k_o r_o^2 \left(\frac{dt}{dr}\right) r = r_o. \qquad (7.3\text{-}6)$$

The quantity $\left(\frac{dt}{dr}\right) r = r_o$ is obtained by differentiating Eq. (7.3-5), and, on substituting and solving for m_o, one obtains

$$m_o = \frac{4\pi r_o r_1 k}{c_p (r_1 - r_o)} \ln\left[1 + \frac{k_o}{k}\frac{c_p}{\lambda}(t_1 - t_o)\right]. \qquad (7.3\text{-}7)$$

Here, k_o is evaluated at t_o while the other physical properties take average values.

An equation very similar to the one above was derived by Godsave [41] in his theoretical analysis of heat transfer in the preflame region around a single burning drop.

Equation (7.3-7) describes evaporation rate, taking into account mass transfer; the carrying away of sensible heat. If mass transfer can be neglected, i.e., $\frac{k_o}{k}\frac{c_p}{\lambda}(t_1 - t_o) \ll 1$, Eq. (7.3-7) reduces to

$$m_o = \frac{4\pi k_o r_o r_1}{\lambda (r_1 - r_o)} (t_1 - t_o), \qquad (7.3\text{-}8)$$

and if $r_1 \gg r_o$, Eq. (7.3-8) further reduces to

$$m_o = \frac{4\pi k_o r_o}{\lambda} (t_1 - t_o). \qquad (7.3\text{-}9)$$

In the various heat transfer equations above, t_o is unknown. In cases in which the air temperature is appreciably higher than the boiling point of the fuel, t_o may be taken as the boiling point without serious error. However, in the general case, t_o must be evaluated with the help of mass transfer considerations and specifically, through the relation between vapor pressure of the drop, p_{f_o}, and the drop temperature.

According to kinetic theory, diffusion in a binary mixture of gases is described [42] as

$$u_f - u_a = \frac{w^2}{w_f w_a} D \frac{d\frac{w_a}{w}}{dr} - \frac{\rho}{\bar{\rho}_f \bar{\rho}_a} \Gamma_f \frac{d\ell n T}{dr} . \qquad (7.3\text{-}10)$$

The assumptions here are small pressure gradients (compared to the magnitude of pressure) and negligible external forces (such as centrifugal fields). The first term on the right describes normal diffusion (where D is the coefficient of molecular diffusion as distinct from the coefficient of eddy diffusion previously discussed) and the second accounts for thermal diffusion. Thermal diffusion can usually be neglected in comparison with normal diffusion. The velocities of fuel vapor and air, u_f and u_a respectively, are relative to a common reference, the average velocity of the mixture. Therefore $u_f - u_a$ is the velocity of fuel with respect to air. In this system the air remains stationary with respect to the drop as the fuel diffuses so that $(u_f - u_a)$ also represents the quantity of direct interest, the velocity of fuel with respect to the drop. The result is then

$$u_f - u_a = \frac{w^2}{w_f w_a} D \frac{d(w_a/w)}{dr} . \qquad (7.3\text{-}11)$$

Fuel velocity may be written in terms of the evaporation rate as

$$u_f - u_a = m_o/\rho_f 4\pi r^2. \qquad (7.3\text{-}12)$$

Assuming the perfect gas law, both mole fractions and densities may be expressed in terms of partial pressures, or

$$\frac{p_f}{p} = \frac{w_f}{w} \text{ and } \frac{p_f}{\rho_f} = \frac{RT}{m_f} .$$

Substituting these relations and Eq. (7.3-12) into (7.3-11), we have

$$m_o = \frac{4\pi r^2 pD m_f}{RD} \frac{d\ell n p_a}{dr} . \qquad (7.3\text{-}13)$$

Equating the mass flow at r and r + dr gives

$$0 = r \frac{d^2(\ell n p_a)}{dr^2} + 2 \frac{d(\ell n p_a)}{dr} . \qquad (7.3\text{-}14)$$

Integrating between r_o and r_1,

$$\ell n p_a = \frac{r_o \ell n p_{a_o} (\frac{r_1}{r} - 1) + r_1 \ell n p_{a_1} (1 - \frac{r_o}{r})}{(r_o - r_1)} \qquad (7.3\text{-}15)$$

Differentiation of this equation and substitution of the resulting expression for $d\ell n p_a/dr$ into Eq. (7.3-13) gives

$$m_o = \frac{4\pi pD m_f r_o r_1}{RT(r_1 - r_o)} \ell n \frac{p_{a_1}}{p_{a_o}} . \qquad (7.3\text{-}16)$$

If the concentration of fuel vapors is small, Eq. (7.3-16) reduces to

$$m_o = \frac{4\pi D \eta_f r_o r_1}{RT(r_1 - r_o)} (p_{a_1} - p_{a_o}), \qquad (7.3\text{-}17)$$

and if it is further assumed that $r_1 >> r_o$, we have

$$m_o = \frac{4\pi D \eta_f r_o}{RT} (p_{a_1} - p_{a_o}) = \frac{4\pi D \eta_f r_o}{RT} (p_{f_o} - p_{f_1}) \qquad (7.3\text{-}18)$$

Numerical values of D may be obtained from, for example, the Gilliland equation [43]. Equation (7.3-18) is the Langmuir equation [44] for slow evaporation of spherical particles in still air. It has been widely verified experimentally for various liquids and solids. However, for very small spheres (the order of 1 to 10 microns or below) at atmospheric pressures, or larger drops at very low pressures (the order of 10 mm of mercury or below) it is in error. The molecular mean free path becomes relatively large and affects the simple mechanisms proposed heretofore. These deviations from the simple theory increase for smaller drops and lower pressures. For these cases a refinement of the equation, proposed by Fuchs [45], has been experimentally confirmed by Bradley [46] showing evaporation rates lower than Langmuir predicts. This refinement is of interest but need not ordinarily be considered in ramjet design.

Equation (7.3-18) is analogous to Eq. (7.3-9) which describes heat transfer to a sphere at low mass transfer rates. Comparison of Eq. (7.3-7) and (7.3-16) show, however, that the heat transfer-mass transfer analogy is not valid at high evaporation (mass transfer) rates. Although the effect of radius is the same, temperature and concentration effects are altered.

In order to solve an actual evaporation problem, one must use both the heat transfer and mass transfer equations. An Antoine equation, for example, is used to relate t_o to p_{f_o} (the vapor pressure of the drop). The constants in this equation (usually $\log p_f = C_1 - C_2/T$) for the fuel in question may be found in, or calculated from, many sources, e.g. [40,47,48].

The importance of mass transfer in lowering the evaporation rate may readily be determined by calculating the ratio of rates with and without taking account of mass transfer. This is done by dividing Eq. (7.3-7) by Eq. (7.3-8), letting $k_o = k$. The ratio so obtained is defined as B and simplifies to

$$B = \frac{\lambda}{c_p(t_1 - t_o')} \ln\left[1 + \frac{c_p}{\lambda}(t_1 - t_o)\right]. \qquad (7.3\text{-}19)$$

In Eq. (7.3-19) t_o is the drop temperature obtained for a given air temperature by neglecting mass transfer in using Eq. (7.3-9) and (7.3-18); however, t_o is the drop temperature obtained for the same air temperature by taking the high-evaporation rate into account using Eq. (7.3-7) and (7.3-16). Figure 7.3-1 presents B as a function of the temperature difference between the air and the average boiling point of an AN-F-32 fuel assuming constant boiling point. It is apparent that mass transfer appreciably lowers evaporation rate at high-temperature differentials between the fuel drops and the air, a common case in ramjet operation. The ideal evaporation rate is reduced 10 per cent at an air temperature equal to the fuel boiling point and 40 per cent at 400°F above the boiling point. Marked along the curve are figures representing the difference between the drop temperature and the boiling point of the fuel. Total pressure has very little effect on this curve and the plot presented is valid from at least 1/3 to 3 atmospheres.

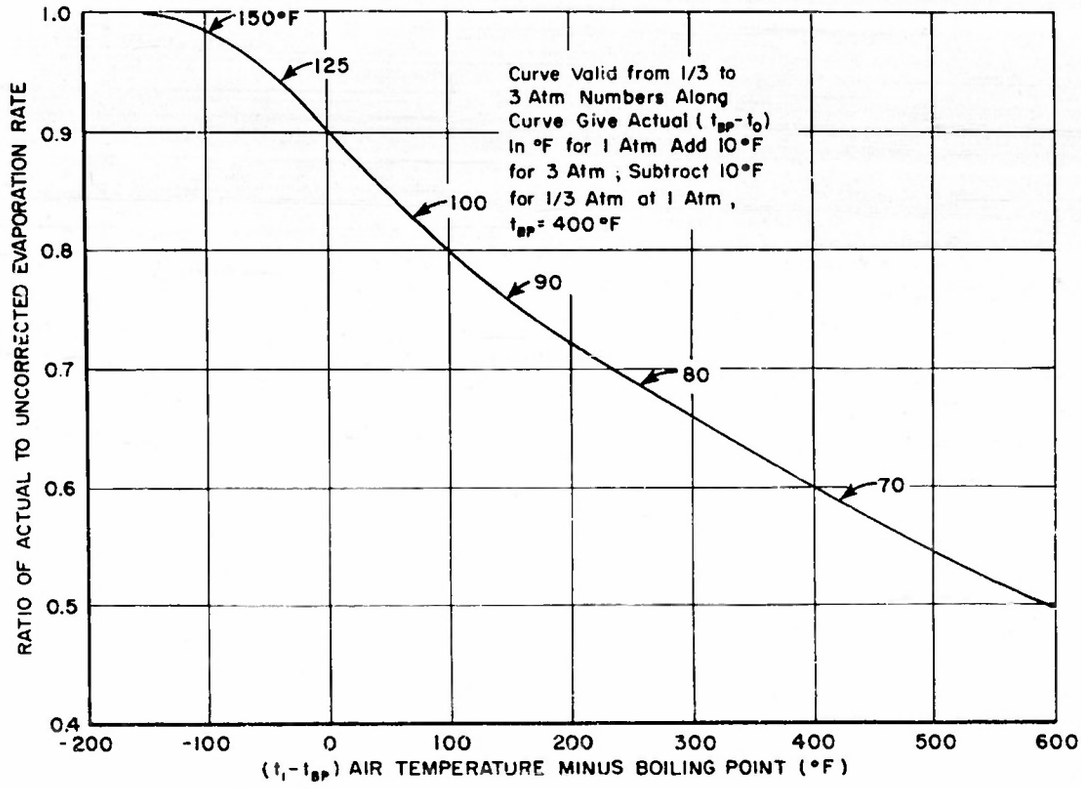

Fig. 7.3-1 REDUCTION OF EVAPORATION RATE OF AN-F-32 CAUSED BY MASS TRANSFER

When air temperatures are very high, t_o may be taken as t_{BP} with negligible error and thus Eq. (7.3-7) may be used directly without the complication of Eq. (7.3-16).

The time required to evaporate any particular drop may be calculated from Eq. (7.3-7) remembering that

$$m_o = \frac{d(\frac{4}{3} r_o^3 \ell)}{d\theta} \qquad (7.3\text{-}20)$$

If we assume $r_1 >> r_o$ and substitute for m_o, $d\theta$ may be separated and the equation directly integrated to give

$$\theta = \frac{c_p \rho_\ell (r_{o_1}^2 - r_o^2)}{2k \ell n \, 1 + \frac{k_o}{k} \frac{c_p}{\lambda} (t_1 - t_o)}, \qquad (7.3\text{-}21)$$

where r_{o_1} is the initial drop radius and r_o the radius at any subsequent time θ. The time required for complete evaporation, when $r_o = 0$, is seen to be dependent on the square of initial drop radius. This indicates the importance of fine atomization to rapid evaporation.

The simultaneous evaporation of a collection of drops of various sizes, the practical case, may be examined next. Assume that the Rosin-Rammler equation [Eqs. (7.1-4) and (7.1-6)] describes the drop size distribution before vaporization begins. Differentiation of this equation gives the mass fraction of material, dY_1, originally found in size range dr_{o_1} with an average size of r_{o_1}

$$dY_1 = \frac{-0.693q}{\bar{r}} \left(\frac{r_{o_1}}{\bar{r}} \right)^{q-1} e^{-0.693\left(\frac{r_{o_1}}{\bar{r}}\right)^q} dr_{o_1}. \qquad (7.3\text{-}22)$$

After the average size of this material has been reduced from r_{o_1} to r_o by evaporation, the fraction of material remaining is

$$\frac{dY}{dY_1} = \left(\frac{r_o}{r_{o_1}} \right)^3 \qquad (7.3\text{-}23)$$

If the quantity $(r_{o_1}^2 - r_o^2)$ is separated from Eq. (7.3-21) and denoted as $(r_{o_1}^2 - r_o^2) = G\theta$, this relation plus that of Eq. (7.3-23) may be combined and r_o eliminated. Then

$$dY = \frac{(r_{o_1}^2 - G\theta)^{3/2}}{r_{o_1}^3} dY_1. \qquad (7.3\text{-}24)$$

Eq. (7.3-22) is used to substitute for dY_1 and then integrating, one obtains

$$Y = \frac{-0.693q}{\bar{r}^q} \int_{\sqrt{G\theta}}^{\infty} r_{o_1}^{q-4} \left(r_{o_1}^2 - G\theta\right)^{3/2} e^{-0.693\left(\frac{r_{o_1}}{\bar{r}}\right)^q} dr_{o_1}, \tag{7.3-25}$$

where Y is the total fraction of the spray unevaporated. Probert [49] has graphically integrated this expression for several values of q; q characterizes the width of distribution, a small q denoting a broad size distribution. Some of his values are reproduced in Fig. 7.3-2 and it may be seen that a broadly distributed spray gives the fastest initial evaporation. However, as evaporation progresses, the rate decreases and the large drops present in a broad spray are quite resistant to evaporation. The practical implication here is that primary ignition of a broad spray in a burner is relatively easy, but complete combustion of the last fraction of fuel is difficult. Such conclusions illustrate the fact that knowledge of the distribution, and not simply some average drop size, is important.

All of the analysis above is complicated in practice by several factors which have not yet been taken into consideration. The most important of these is the relative velocity between the fuel drop and the air stream. Such a relative velocity occurs in two ways. The fuel drops, immediately upon injection, must be accelerated to the air-stream velocity. Also, once reaching the mean-stream velocity they are subject to turbulenc fluctuations which cannot be exactly followed by the drops (Section 7.2). Effects like these cause evaporation rate to be higher than that predicted by simple conduction in still air.

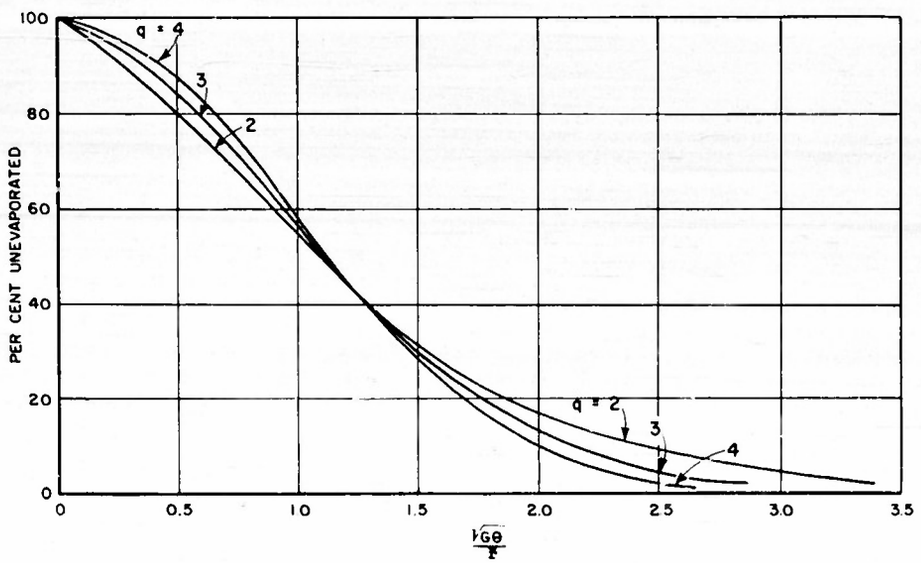

Fig. 7.3-2 EVAPORATION OF SPRAYS WITH EQUAL MASS MEDIAN DROP RADIUS

This increase of evaporation rate caused by relative velocity may be handled conveniently by means of the group $r_1/(r_1 - r_o)$ in Eqs. (7.3-7) and (7.3-16). In still air, r_1 is very large, even infinite, so that the group above takes the value of 1. However, as relative velocity increases and $r_1 \longrightarrow r_o$, the group takes on larger values and increases the evaporation rate accordingly. Ranz and Marshall [50] show that this group may be correlated in the following manner for Nusselt numbers from 2 to 200

Heat transfer: $$\frac{2r_1}{r_1 - r_o} = Nu = 2.0 + 0.60\ Pr^{1/3}\ Re^{1/2}. \quad (7.3\text{-}26)$$

Mass transfer: $$\frac{2r_1}{r_1 - r_o} = Nu' = 2.0 + 0.60\ Sc^{1/3}\ Re^{1/2}. \quad (7.3\text{-}27)$$

In these equations Pr, Re, and Sc are the dimensionless Prandtl, Reynolds, and Schmidt numbers respectively, and Nu and Nu' are the Nusselt numbers for heat and mass transfer respectively. The data for Eqs. (7.3-26) and (7.3-27) were taken at low-evaporation rates so that the velocity of the evaporated material could be neglected. Data at high rates are scant; however, as a first approximation, it can be assumed that the effective film thickness ($r_1 - r_o$) will not change. It is known [51] that in the case of a flat surface, mass transfer away from the surface thickens the boundary layer, increasing r_1, and giving lower-evaporation rates.

In order to calculate the Nusselt numbers, the Reynolds number of the drop must be known. This depends on the relative velocity between the drop and the air stream. Such velocities may be calculated, in the case of a drop starting from rest, by a force balance. The drag on the drop, a sphere, is equated to the product of its mass and acceleration. Thus, using Langmuir and Blodgett's [25] drag equation:

$$6\pi\mu\Delta u r_o \left(1 + 0.197\ \mathrm{Re}^{0.63} + 2.6 \times 10^{-4}\ \mathrm{Re}^{1.38}\right) = \frac{4}{3}\pi r_o^3\ \rho_\ell \frac{d\Delta u}{d\theta} \qquad (7.3\text{-}28)$$

For ramjet conditions, the third term in parentheses may be neglected and Eq. (7.3-28) integrated to give

$$\frac{\mathrm{Re}}{\mathrm{Re}_o}^{0.63} \left(\frac{1 + 0.197\ \mathrm{Re}_o^{0.63}}{1 + 0.197\ \mathrm{Re}^{0.63}}\right) = e^{\frac{-2.84\mu\theta}{r_o^2 \rho_\ell}} \qquad (7.3\text{-}29)$$

Equation (7.3-29) describes the Reynolds number, Re, of a single spherical drop starting from rest (at $\theta = 0$), with an initial Reynolds number of Re_o, after any time θ. At high

relative velocities the drops are probably deformed somewhat and thus have a higher drag and acceleration. Close to the injection point, the drops are also close together and there is some error in Eq. (7.3-29) because the air in an accelerating spray will be slowed down relative to air outside the spray. However, Eq. (7.3-29) is of sufficient accuracy for illustrative purposes.

If a 45 micron drop of kerosene is accelerated from rest in a 300 ft/sec air stream at one atmosphere, the drop travels 1.2 feet before reaching 97 per cent of the main stream speed. At this point the relative velocity is equal to the turbulent intensity in the center of a duct with fully developed pipe turbulence and Re would be six. The distance above assumes no evaporation, i.e., constant size.

The response of a drop to turbulent fluctuation can also be estimated. For the same drop as above, assuming an intensity of 3 per cent, the maximum Re of the drop caused by turbulence would be 4.7. This would increase the evaporation rate, by Eq. (7.3-7), 60 per cent.

The discussion above indicates the importance of relative air velocity to evaporation rate. Other effects must also be considered. For example, a cold fuel droplet must be heated to its equilibrium surface temperature before appreciable evaporation occurs.

Tanasawa and Kobyasi [52] considered such a case and presented a chart for solving the equation, modified here, for the time, θ, required to come to equilibrium surface temperature, t_o:

$$\left(\frac{t_a - t_o}{t_a - t_f}\right) = 2 \sum_{S=1}^{\infty} \frac{\exp\left(-v_s^2 \alpha_\ell \theta / r_o^2\right)}{\frac{Nuk_a}{2k_\ell} - 1 + v_s^2 \frac{Nuk_a}{2k_\ell}} , \qquad (7.3\text{-}30)$$

where v_s is a root of the equation $v_s = \left(1 - \frac{Nuk_a}{2k_\ell}\right) \tan v_s$, and α is the thermal diffusivity of the liquid. It is important to remember that evaporation of the drop during this heating period, and convection within the drop, have been neglected. Otherwise, equilibrium temperature could not be reached in finite time. The time, θ can be separated out in the form $\theta = C \frac{r_o^2}{\alpha_\ell}$ where C has been expressed graphically in Fig. 7.3-3 as a function of $(t_a - t_o)/(t_a - t_f)$ and some average Nu must be determined using Eqs. (7.3-29) and (7.3-26). The importance of this heat conduction to the liquid drop depends on the ratio of specific to latent heats. Kerosene, for example, has a latent heat of about 110 BTU/lb and a specific heat of about 0.55 BTU/lb^{o}F. Obviously, if the fuel must be heated 200^{o}F from its initial to equilibrium temperature, the sensible heat involved is equal to that required to evaporate the entire drop. In such a case, this sensible heat to the drop cannot be neglected. In practice however, drops are usually injected from rest into a high velocity air stream. The result is extremely high rates of initial heat transfer which drop off very rapidly. Thus the cold fuel quickly comes to equilibrium temperature as it is accelerated. The evaporation rate then drops off until it approaches constancy as the main stream velocity is reached. The 45 micron drop of kerosene injected from rest into a 300 ft/sec air stream at 400^{o}F will theoretically travel less than an inch before equilibrium surface temperature is reached.

Other considerations to be taken into account are the effect of changing drop composition (and thus surface temperature) as evaporation progresses, the effect of air temperature lowering as sensible heat of the air is used for vaporization, and the suppression of evaporation by the building up of a fuel vapor partial pressure in the air. These effects are usually

negligible but can be accounted for, if necessary, by manipulation of equations already given.

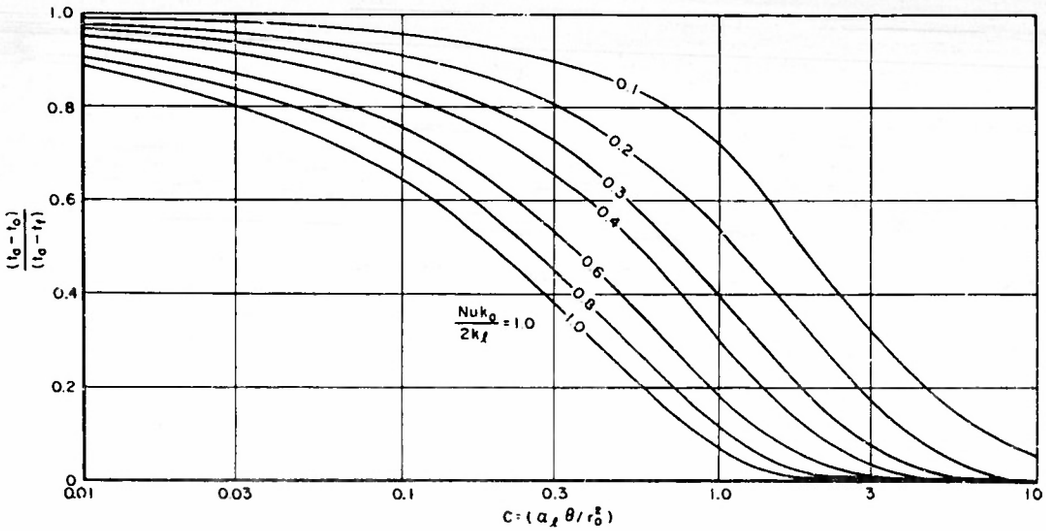

Fig. 7.3-3 HEATING OF A LIQUID DROP TO EQUILIBRIUM SURFACE TEMPERATURE

Experimental Evaporation Data

Experimental evaporation data in the range of interest to ramjet engine designers are very limited. Geometries and physical properties are often difficult to either control or measure. However, a few measurements of direct interest are available as are some data taken under idealized conditions, useful for evaluation of the theoretical analysis above.

There have been several investigations of the evaporation, at low rates, of single spheres (of iodine, naphthalene, water, etc.) in still air. These data validate Eq. (7.3-18), above. Some more recent work by Ingebo [53] studied the high-

rate evaporation of nine pure liquids from a 0.688 cm sphere in moving air. The Reynolds number range was about 600 to 6000. The following equation was found to best correlate the data:

$$m_o = \frac{k_a(t_1 - t_o)}{\lambda} 2\pi r_o \left(\frac{k_a}{k_f}\right)^{1/2} \left(2 + 0.303 Re^{0.6} \cdot Sc^{0.6}\right). \qquad (7.3\text{-}31)$$

It is apparent from Eq. (7.3-31) that the effect of mass transfer on the temperature gradient is not accounted for and therefore the equation, although representing the data fairly well, is an empirical one for the conditions investigated.

Godsave [41] has studied the combustion of single liquid drops in still air using three commercial hydrocarbon fuels and ten pure aromatic hydrocarbons. The problem of combustion of single drops reduces to a study of the evaporation of the drop subject to very high temperature differentials. Using a photographic technique, Godsave determined the rate of change of drop size with time during combustion. His results can be only qualitatively interpreted in the light of the theory developed because of lack of exact knowledge of all of the physical properties and geometries involved. However, those variables which can be separated confirm the theoretical analysis.

It has been shown previously that evaporation may be represented from Eq. (7.3-21) by the equation

$$\left(r_{o_1}^2 - r_o^2\right) = G\theta, \qquad (7.3\text{-}32)$$

where G is the so-called evaporation constant. This equation is applicable if the mass rate of evaporation is directly proportional to drop radius. Godsave found this to be so for all the liquids investigated (ranging from naphtha to diesel oil)

with the constant, G, varying between about 1.8×10^{-6} and 2.7×10^{-6} ft^2/sec. It was further determined that fuel volatility had little effect on this constant (which is to be expected at very high temperature differentials); also, the constant decreased as latent heat of vaporization of the fuel increased. All of these results tend to confirm the concept of a heat transfer mechanism in evaporation as outlined above.

Gross effects in the evaporation of a fuel spray have been studied at the University of Michigan [23] and at the Esso Laboratories [29]. At Michigan, hexane was sprayed through a hollow-cone atomizing nozzle downstream in a 50-75 ft/sec air stream. Various upstream turbulence inducers were used to vary the turbulent intensity of the moving air. The results pertinent to this work were that, at a given fuel rate and distance downstream, the degree of evaporation increased with both increasing turbulent intensity and increasing air velocity.

The effect of velocity found at Michigan is confirmed by work at Esso which shows, Fig. 7.3-4, that for both constant fuel rates and constant air/fuel ratios evaporation increases (at a given station, 17 inches downstream) as air velocity does. In these tests, a narrow-cut fuel ($t_{BP} = 328^{\circ}F$) was injected contrastream at low velocity through an injection tube. Air pressure and temperature were one atmosphere and $235^{\circ}F$ respectively. The effect of air velocity probably results from better atomization (smaller drops) of fuel and from better heat and mass transfer coefficients (higher initial relative velocity and higher turbulent intensities).

The influence of fuel type is illustrated in Fig. 7.3-5 which compares the evaporation in air at atmospheric pressure and $200^{\circ}F$ of naphtha (average boiling point about $185^{\circ}F$) and AN-F-32 (average boiling point about $385^{\circ}F$). These data were taken at an air velocity of 500 ft/sec, at equal fuel rates,

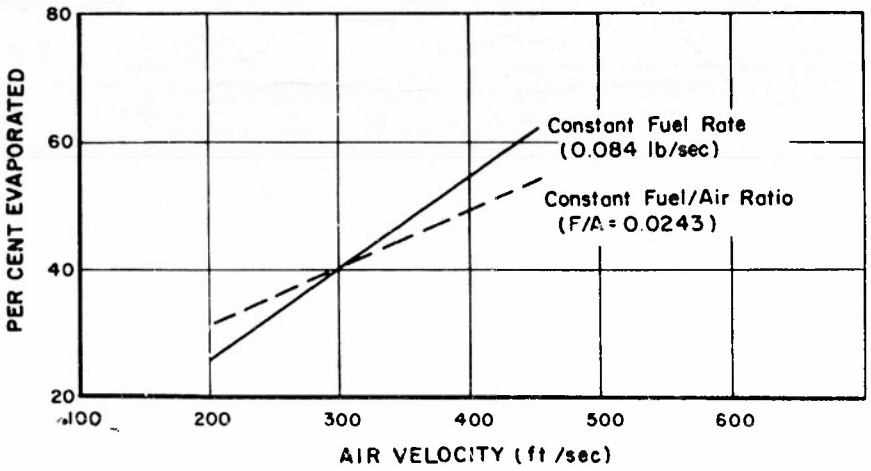

Fig. 7.3-4 EFFECT OF AIR VELOCITY AND FUEL RATE ON EVAPORATION

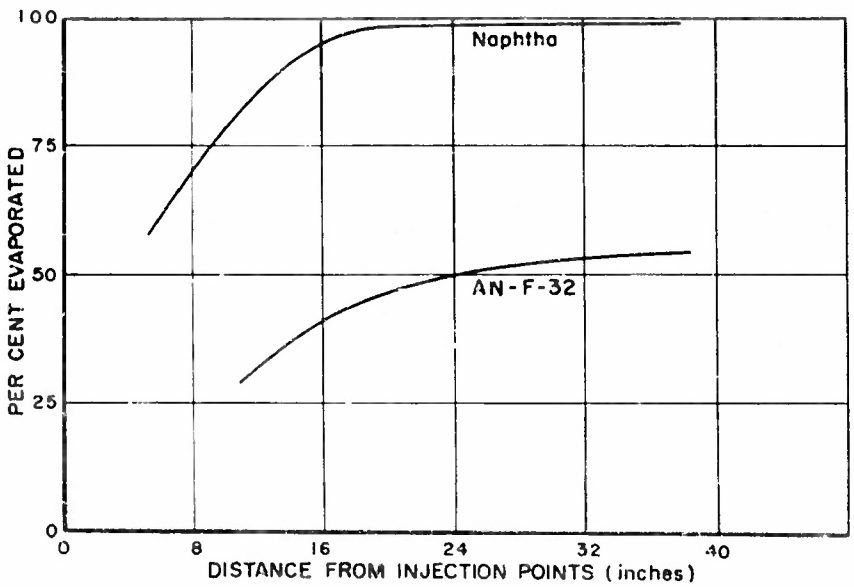

Fig. 7.3-5 EFFECT OF SURVEY DISTANCE AND FUEL TYPE ON EVAPORATION

and under conditions such that 95 per cent of the kerosene would vaporize at equilibrium. It is obvious that the naphtha, whose boiling point is 15°F below the air temperature evaporates much more readily than the kerosene, whose boiling point is 185°F above the air temperature. In fact, 95 per cent of the naphtha evaporates within only 16 inches of the injection point. However, in both cases it is of interest to note that the high initial-evaporation rates rapidly fall off. This is the result of several effects--the residue of initially large drops, the decrease of air temperature as evaporation progresses, the increase of drop temperature by vaporization of the lower-boiling fuel components, and the rapid approach of drop velocity to air stream velocity (thus reducing relative velocity and heat transfer).

In other similar tests, increase of air temperature or fuel-injection temperature was found, as expected, to increase the degree of evaporation, other conditions held constant. These tests were run at an air velocity of 300 ft/sec and atmospheric pressure, again using a narrow-cut fuel with an average boiling point of 328°F. Measurements made 17 inches downstream of the injection point (a simple contrastream tube) gave the following results. For a constant fuel temperature (90°F) and varying air temperature (before mixing),

t_a (°F)	190	235	267
per cent evaporated	30	44	52

When air temperature was held constant (235°F) and fuel injection temperature varied,

t_f (°F)	90	170	200
per cent evaporated	44	58	62

In these experiments, the data can be roughly summed up by noting that a 1 per cent increase (based on total fuel) in evaporation occurred for a $4^{\circ}F$ rise in fuel temperature or a $6^{\circ}F$ rise in air temperature.

From other data of this type, it has been tentatively concluded [29] that pressure (in the range of 1/3 to 1 atmosphere) does not significantly affect evaporation rate. This conclusion assumed that, for all pressures, the fuel is injected at a temperature such that the differential between injection temperature and average boiling point at the operating pressure is a constant. Furthermore, the air temperature is adjusted for pressure such that the same equilibrium vaporizations are possible.

As may be seen from the discussion above, the existing experimental data qualitatively confirm the theoretical analysis. Considerably more data are needed for quantitative confirmation. However, the purpose of this section has not been to provide rigid design procedures for fuel evaporation. Rather it has been to point out the major variables affecting evaporation and the order of magnitude of change to be expected when altering those variables.

NOMENCLATURE

The following nomenclature has been used throughout, with the units noted, unless otherwise indicated in the text.

Symbol	Definition	Unit
A	cross-sectional area	ft^2
A_A	arithmetic average of A_S and A_I	ft^2
A_I	duct area at injection station	ft^2
A_S	duct area at survey station	ft^2
A/F	mass ratio of air to fuel	--
a	size constant in Nukiyama-Tanasawa equations (7.1-5, 7.1-7)	--
B	ratio of actual to uncorrected evaporation rate	--
b	$3\pi\mu d_o/m$	sec^{-1}
C	transient heating constant, $\alpha\ell\theta/r_o^2$	--
C_E	vapor-liquid distribution constant	--
c_o	constant pressure heat capacity	BTU/lb ^oF
D	molecular diffusion coefficient	ft^2/sec
$\bar{d}$	mass mean drop diameter for spray distribution	ft
d_c	collector diameter	ft
d_o	drop diameter	ft
E	eddy diffusion coefficient	ft^2/sec
E_o	eddy diffusion coefficient of a gas	ft^2/sec
f	local mass ratio of fuel to air	--

G	evaporation constant (Eq. 7.3-32)	ft^2/sec
H	molar enthalpy	BTU/lb mole
h	heat transfer coefficient	BTU/ft^2 sec ^oF
I_o	modified Bessel function of first kind, zero order	--
K	$uR_o^2/4Ex$	--
k	thermal conductivity	BTU/ft sec ^oF
k_g	mass transfer coefficient; $k_g = m_o/\mathcal{M}_f \pi r_o^2 \Delta p_f$	--
L	R/M	--
ℓ	scale of turbulence	ft
ℓn	$\log_e$	--
M	radius of disk source	ft
$\mathcal{M}$	molecular weight	--
m	mass of drop	lb
m_o	mass evaporation rate	lb/sec
Nu	Nusselt number for heat transfer ($d_o h/k$)	--
Nu'	Nusselt number for mass transfer ($d_o k_g \mathcal{M}_f p_f/\rho_f D$)	--
n	number of components	--
P	$uM^2/2Ex$	--
Pr	Prandtl number ($c_p \mu/k$)	--
p	static pressure (partial pressure with subscript)	atm
Q	heat	BTU
q	distribution constant in distribution equation	--

R	universal gas constant (0.729)	ft^3 atm/ lb mol ^oR
R	radial distance from injection source axis to survey point	ft
$\bar{R}$	R/R_o	--
Re	Reynolds number ($d_o \Delta u \rho / \mu$)	--
R_i	fuel jet radius	ft
R_o	radius of ring source	ft
r	distance perpendicular to flow axis; also, radial distance	ft
$\bar{r}$	mass mean drop radius for spray distribution	ft
r_m	mass mean duct radius for fuel distribution	ft
r_s	surface/volume mean radius for spray distribution	ft
S	specific gravity referred to water	--
Sc	Schmidt number ($\mu/\rho D$)	--
s	drop spacing (in drop diameters)	--
T	absolute temperature	^oR
t	temperature	^oF
t'_o	uncorrected drop temperature	^oF
$\Delta t'$	temperature differential between curve and its reference line at constant per cent distilled	^oF
t_{40}	temperature at 40 per cent distilled on flash curve	^oF
t^*_{50}	temperature at 50 per cent distilled on reference line	^oF
u	velocity	ft/sec

$\bar{u}$	velocity of turbulent fluctuation	ft/sec
u_o	peak velocity of sinusoidal fluctuation	ft/sec
V	volume	ft^3
v_s	a root of $v_s = \left(1 - \frac{Nuk_a}{2k\ell}\right) \tan v_s$	--
W_a	mass velocity of air	lb/ft^2 sec
W_f	rate of fuel injection	lb/sec
w	moles of material	lb moles
x	distance along flow axis	ft
Y	mass fraction of material	--
y	dimensionless function of drop diameter distribution probability	--
Z	displacement of drop	ft
Z_m	maximum value of Z	ft
Z_o	maximum amplitude of sinusoidal fluctuations	ft
α	thermal diffusivity ($k/\rho c_p$)	ft^2/sec
β	spray cone angle	radians
Γ_f	thermal diffusion constant	--
Γ	Gamma function, $\Gamma(n) = \int_o^\infty x^{n-1} e^{-x} dx$, $\Gamma_\beta(n) = \int_o^\beta x^{n-1} e^{-x} dx$	--
γ	$-m_o c_p / 4 kr_o$	--
θ	time	sec

λ	latent heat of vaporization	BTU/lb
μ	viscosity	lb/ft sec
ρ	density	lb/ft^3
σ	surface tension	dynes/cm
ϕ	ring source function (Eq. 7.2-10)	--
Ψ	disk source function (Eq. 7.2-11)	--
ℓ	collection efficiency parameter, $\rho_\ell d_o / 9 \rho_a d_c$	--
ω	frequency	radians/sec

Subscripts
(unless defined above)

a	air
BP	boiling point
e	equilibrium
f	fuel (total)
HC	hydrocarbon
i	any particular component
ℓ	liquid (fuel)
v	vapor (fuel)
o	drop surface conditions
1	initial conditions; also, bulk stream conditions
2	final conditions

APPENDIX

Empirical Method for Calculating Equilibrium Vaporization

The laboriousness of the enthalpy calculation procedure described in Section 7.3 led to the development of several empirical methods for determining equilibrium (flash) vaporization. In the method below, the only information about the fuel required is the ASTM distillation curve and specific gravity (at 60°F). The notation used is the same as that for Chapter 7.

From the ASTM distillation curve the slope of a distillation reference line (DRL) is calculated (in °F/per cent distilled) where the DRL is the straight line through the 10 per cent and 70 per cent points on the ASTM curve. Using this slope and Fig. 7A-1, the slope of a flash reference line (FRL) is determined. Next, the temperature at the 50 per cent point (t^*_{50}) on the DRL is calculated and from Fig. 7A-1 the temperature correction, t^*_{50} (DRL) - t^*_{50} (FRL), is read. The FRL is now established inasmuch as its slope and one point on it (t^*_{50} [FRL], the temperature at the 50 per cent point) are known. Temperature differentials [$\Delta t'$ (Dist.)] between the ASTM curve and the DRL are calculated at (at least) each 10 per cent point along the abscissa. Each $\Delta t'$ (Dist.) is then multiplied by the factor $\Delta t'$ (Flash)/$\Delta t'$ (Dist.), read from Fig. 7A-2, to give a new differential, $\Delta t'$ (Flash), which is added, at the appropriate per cent distilled, to the FRL. The Δt's may be positive or negative but their ratio is always positive. The new curve obtained by adding $\Delta t'$ (Flash) to the FRL is the flash vaporization curve (FVC) and this curve represents the equilibrium vaporization of the fuel for

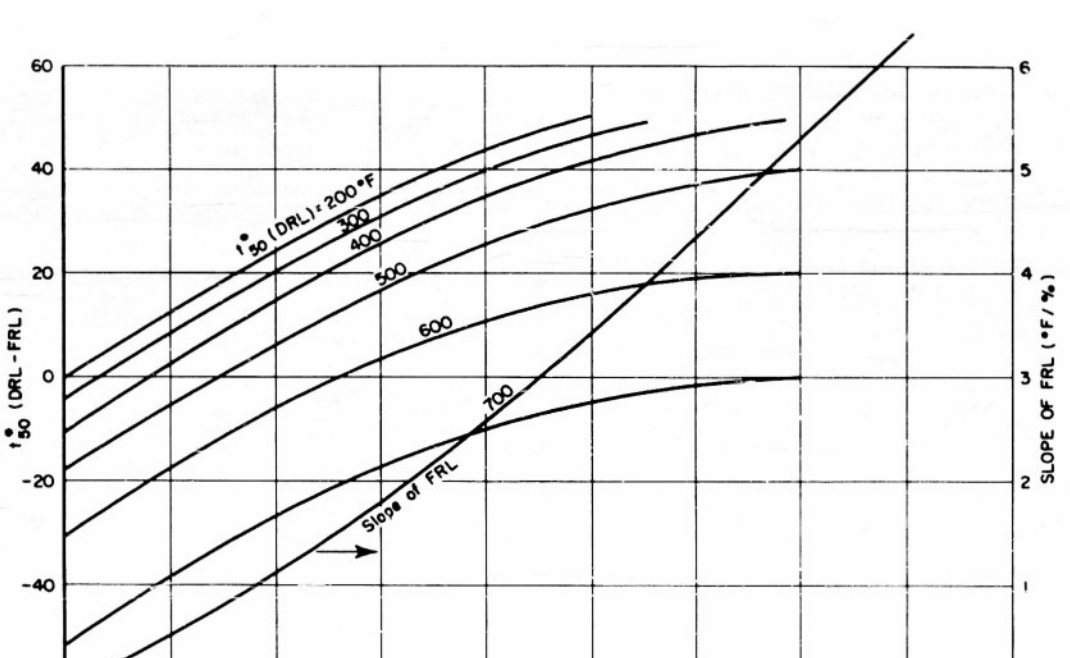

Fig. 7A-1 PREDICTION OF FRL FROM DRL

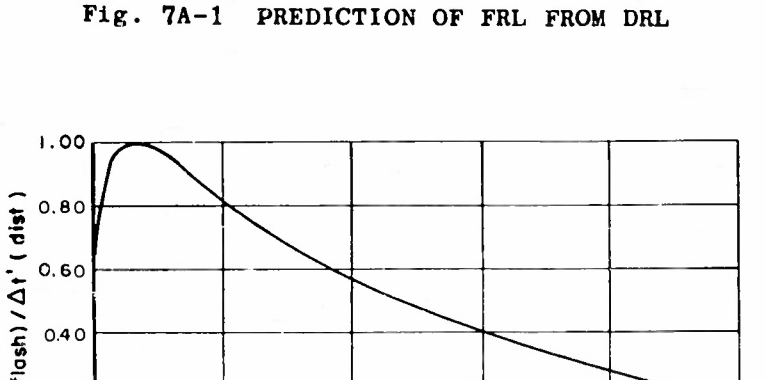

Fig. 7A-2 PREDICTION OF FLASH CURVE FROM FRL

a hydrocarbon partial pressure in the vapor of one atmosphere. For any given temperature ordinate, the abscissa is the volume fraction of fuel that will vaporize at equilibrium.

During evaporation of fuel into air the only pressure information usually known is the static pressure--the sum of the partial pressures of air and hydrocarbon. The partia pressure of the hydrocarbon is only a small fraction (a few per cent at most) of the static pressure because of the high mass ratio of air to fuel and because of the mucl lower molecular weight of air relative to most fuels. The FVC above must then be converted to a new curve corresponding to this lower hydrocarbon partial pressure. The first step in this conversion is calculation of the average molecular weight (m) of the vapor versus per cent vaporized. This curve is approximated by a straight line connecting the 0 per cent and 100 per cent points. The 100 per cent point is located by means of Fig. 7A-3, reading the molecular weight from the mean average boiling point of the total fuel as abscissa and specific gravity as parameter. This "mean average" boiling point is obtained in the insert of Fig. 7A-3 from the volume average boiling point (the average ordinate of the ASTM curve) and the slope of the DRL.

The "0 per cent" point is located as to temperature by extrapolating the DRL to 0 per cent distilled. Its specific gravity is established by the intersection of this temperature on Fig. 7A-3 with a curve parallel to the dotted reference curve indicated and passing through the previously located 100 per cent point. The molecular weight can then be read and a molecular weight-per cent vaporized curve drawn.

The remainder of the calculation is a trial procedure. Assume a certain mass fraction vaporized (Y_v), a static pressure (p), and an over-all air/fuel ratio (A/F). If m is the average molecular weight of the vaporized hydrocarbon fraction,

the hydrocarbon partial pressure is

$$p_{HC} = \frac{Y_v/m}{A/F/28.9 + Y_v/m} . \qquad (7A-1)$$

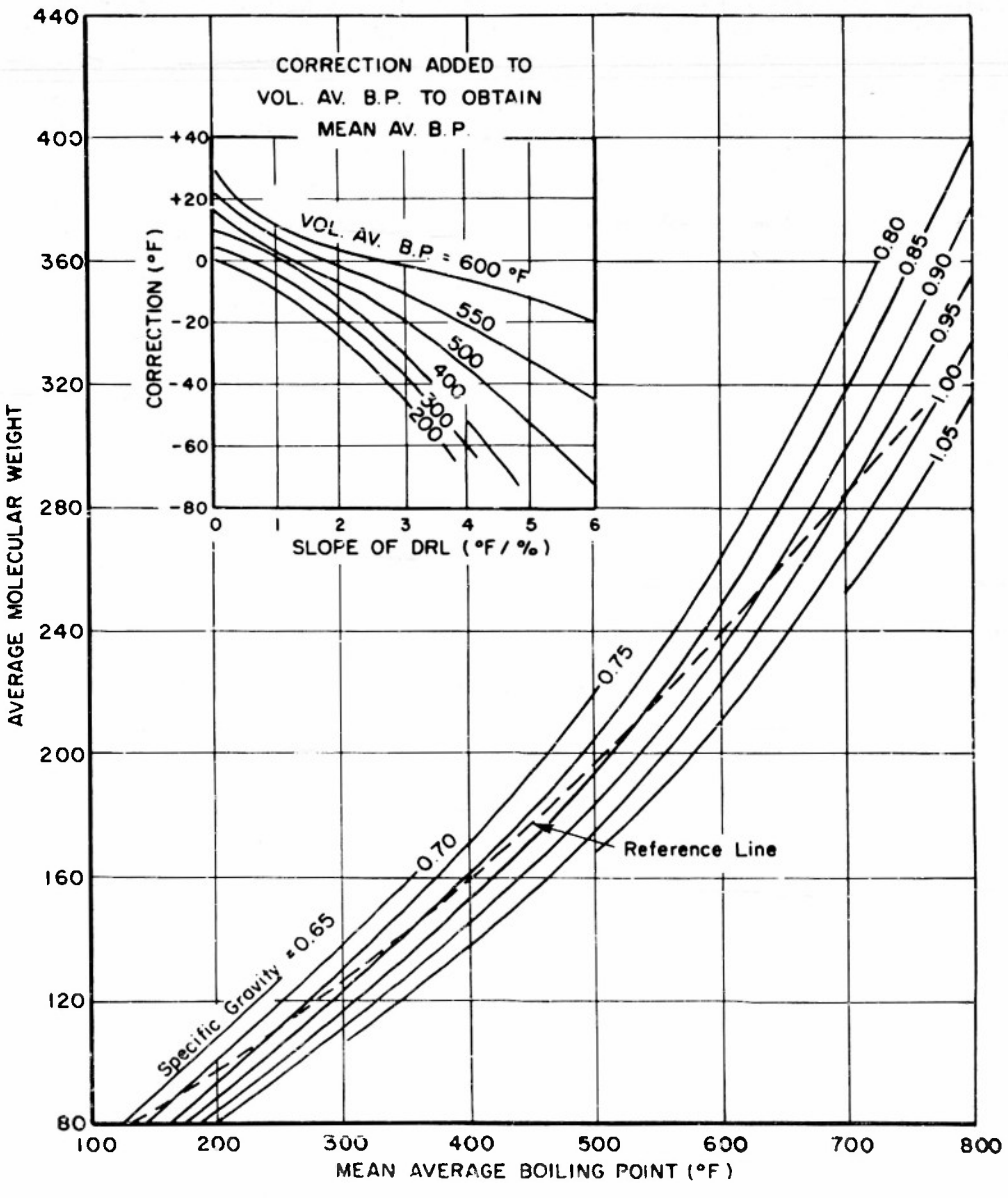

Fig. 7A-3 AVERAGE MOLECULAR WEIGHT OF HYDROCARBON FRACTIONS

Read next the temperature of the 40 per cent (t_{40}) on the FVC. From Chapter 5 determine the temperature lowering that must occur to have a hydrocarbon normally boilint at t_{40} exert a vapor pressure equal to p_{HC}. Subtract this differential from the temperature on the FVC corresponding to the assumed Y_v. This new temperature (t_e) is the temperature at equilibrium. From a heat balance, the air temperature (t_a) before mixing can be calculated if the fuel temperature before mixing (t_f) is known.

$$\frac{A}{F} c_{p_a} (t_a - t_e) = c_{p_f} (t_e - t_f) + Y_v \lambda t_e \qquad (7A\text{-}2)$$

Average fuel heat capacity can be found from the equation given by Hougen and Watson [A1], in modified units, as follows:

$$c_{p_f} = \left[\frac{0.5 \sqrt[3]{T_{BP}}}{S} + 0.41\right]\left[0.187 + \frac{0.181}{S} + 10^{-3}\, t\left(0.349 + \frac{0.166}{S}\right)\right] \qquad (7A\text{-}3)$$

With less than 1 per cent maximum error, the heat capacity of air can be expressed (below 600°F) by

$$c_{p_a} = 0.240 + 1.6 \times 10^{-5} t. \qquad (7A\text{-}4)$$

Latent heats may be estimated from Fig. 7A-4.

From Eq. (7A-2), t_a may be separated and solved for. Inasmuch as t_a will usually be a given condition, Y_v must be adjusted by trial to give the proper t_a. The fraction vaporized can then be plotted as a function of t_a for various parameters of A/F and p.

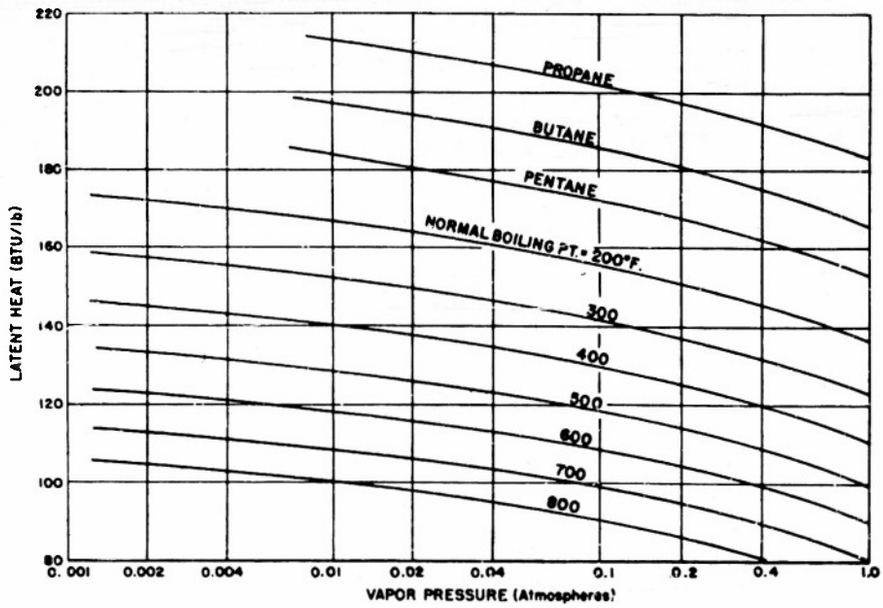

Fig. 7A-4 LATENT HEAT OF VAPORIZATION OF PARAFFIN HYDROCARBONS

Although the calculation method above seems quite complex, it can be performed fairly rapidly with good accuracy and is the simplest procedure known to the authors for reliable determination of equilibrium vaporization.

Illustrative Calculation

Assume an AN-F-32 fuel, specific gravity of 0.813, ASTM distillation as follows.

Distillation (per cent)	Initial	2	5	10	20	30	40	50	60	70	80	90	95	Final
^{o}F	314	342	349	355	362	370	380	390	401	414	433	458	480	504

The conditions for evaporation will be assumed as an A/F ratio of 22, a static pressure (p) of 380 mm (0.5 atm), and inlet fuel temperature of $80^{o}F$.

Slope of DRL = $(414-355)/60 = 59/60 = 0.99^{o}F/\%$

From Fig. 7A-1, slope of FRL = $0.52^{o}F/\%$

t^{*}_{50} (DRL) = $355 + 40 \times 59/60 = 394^{o}F$

From Fig. 7A-1, t^{*}_{50} (DRL) - t^{*}_{50} (FRL) = $+2^{o}F$

Therefore t^{*}_{50} (FRL) = $392^{o}F$

In Table 7A-1, columns (I) and (II) are taken from the ASTM distillation curve. Column (III) is calculated from points along the DRL. Column (IV) is (III) minus (II). The values of (V) are read from Fig. 7A-2 using the abscissa of column (I). Multiplication of (V) and (IV) gives (VI). Column (VII) is calculated from the FRL slope and t^{*}_{50} (FRL). Finally, column (VIII), the atmospheric flash vaporization curve, is (VII) minus (VI). Proceed to calculation of p_{HC} as follows.

Volume average boiling point of total fuel (integrating under ASTM curve) = $398^{o}F$.

From insert of Fig. 7A-3, mean average boiling point = 398 + 0 = 398°F.

From Fig. 7A-3, average molecular weight of entire fuel, 100 per cent vaporized, (boiling point = 398°F and gravity = 0.813) = 158.

From Fig. 7A-3, average molecular weight at "0 per cent" vaporized (boiling point = 345°F and gravity = 0.80) = 139.

For first trial assume $Y_v = 0.5$; therefore $\mathcal{M} = 148$, from curve of molecular weight versus fraction vaporized.

Table 7A-1

(I) Dist (per cent)	(II) ASTM	(III) DRL	(IV) Δt' (Dist)	(V) Δt' (Flash) ÷ Δt' (Dist)	(VI) Δt' (Flash)	(VII) FRL	(VIII) FVC
0	314	345	31	0.50	16	366	350
2	342	347	5	0.88	4	367	363
5	349	350	1	0.99	1	369	368
10	355	355	-	-	-	371	371
20	362	365	3	0.82	2	376	374
30	370	375	5	0.67	3	382	379
40	380	384	4	0.56	2	387	385
50	390	394	4	0.49	2	392	390
60	401	404	3	0.41	1	397	396
70	414	414	-	-	-	402	402
80	433	424	-9	0.28	-3	408	411
90	458	434	-24	0.23	-6	413	419
95	480	439	-41	0.20	-8	415	423
100	504	443	-61	0.18	-11	418	429

From Eq. (7A-1), $p_{HC} = \frac{(0.5/148)}{(22/28.9 + 0.5/148)} = 380 = 1.68$ mm Hg

From FVC, $t_{40} = 385^{\circ}F$.

From Chapter 5.4, the temperature at which a hydrocarbon normally boiling at $385^{\circ}F$ has a vapor pressure of 1.68 mm = $111^{\circ}F$.

Lowering of temperature = $385 - 111 = 274^{\circ}F$.

From FVC, temperature at $Y_v = 0.5$ is $390^{\circ}F$.

$t_e = 390 - 274 = 116^{\circ}F$.

Solve for t_a from Eq. (7A-2)

$$22\, c_{p_a}(t_a - 116) = c_{p_f}(116 - 80) + 0.5\lambda_{116}$$

From Eq. (7A-4), $c_{p_a} \cong 0.241$ (estimating t_a as $140^{\circ}F$).

From Eq. (7A-3), $c_{p_f} = 0.461$ (using S = 0.81 and $t_{BP} = 827^{\circ}R$).

From Fig. 7A-4, $\lambda_{116} = 149$ (using a vapor pressure of 1.68/760 atmospheres and a normal boiling point, the volume average boiling point on the ASTM curve and $t_a = 133^{\circ}F$.

To obtain other values of t_a assume various values of Y_v and proceed as above until the desired range of t_a is covered. Repeat for other conditions of A/F, t_f, and/or p [54].

REFERENCES

1. Scheubel, F. N., Wissenschaftliche Gesselschaft fur Luftfahrt (WGL) Jahrbuch, 140, (1927).

2. Erken, Brack, and Zoeller, Massachusetts Institute of Technology M. S. Thesis, 1948.

3. Castlemen, R. A., Jr., Bur. Standards J. Research, 6, 396 (1931).

4. Rayleigh, Proc. London Math. Soc., 10, 4 (1879) (Sci. Papers Art. 58) Chap. XX.

5. Weber, C., Z. Angewandte Math. und Mech., 11, 136 (1931).

6. David, W.A.L., Bull. Entomol. Research, 37, (1946).

7. Kuehn, R., Atomization of Liquid Fuels, NACA TM 329-331, 1925.

8. Gelalles, A. G., Effect of Orifice Length - Diameter Ratio on Fuel Sprays for Compression - Ignition Engines, NACA TR 402, 1931.

9. Nukiyama, S. and Tanasawa, Y., Trans. Soc. Mech. Engrs. (Japan), 4, 86 (1938); 5, 138 (1939); 6, 63, 68, II-7, II-8 (1940).

10. Lane, W. R., Ind. Eng. Chem., 43, 1312 (1951).

11. Bevans, R. S., Mathematical Expressions for Drop Size Distributions in Sprays, Conference on Fuel Sprays, University of Michigan, March 30-31, 1949.

12. Mugele, R. A., and Evans, H. D., Ind. Eng. Chem., 43, 1317 (1951).

13. Rupe, J. H., A Technique for Investigation of Spray Characteristics of Constant Flow Nozzles, Conference on Fuel Sprays, University of Michigan, March 30-31, 1949.

14. May, R. K., J. Sci. Instruments, 22, 187 (1945).

15. Stoker, R. L., J. Appl. Phys., 17, 243 (1946).

16. Doble, S. M., Proc. Inst. Mech. Eng. England, 157, 103 (1947).

17. Giffen, E. and Muraszew, A., Fuel Injection in Internal Combustion Engines, Third (Aug. 1948) and Fourth (Sept. 1948) Reports, Motor Industry Research Association, Middlesex (Great Britain).

18. Brun, R. J., et al, An Instrument Employing a Coronal Discharge for the Determination of Droplet-Size Distribution in Clouds, NACA TN 2458, 1951.

19. Levine, J. and Kleinknecht, K. S., Adaptation of a Cascade Impactor to Flight Measurement of Droplet Size in Clouds, NACA RM E51G05, 1951.

20. Joyce, J. R., The Wax Method of Spray Particle Size Measurement, Tech. Report, No. I.C.T./7, Shell Petroleum Co., Ltd., August 1946.

21. Longwell, J. P., Sc. D. Thesis, M.I.T. (1941).

22. Sauter, J., Determining Size of Drops in Fuel Mixture of Internal Combustion Engines, Trans. in NACA TM 390 (1926).

23. Fledderman, R. G. and Hanson, A. R., The Effects of Turbulence and Wind Speed on the Rate of Evaporation of a Fuel Spray, University of Michigan, CM-667, June 20, 1951.

24. Geist, J. M., et al, Ind. Eng. Chem., 43, 1371 (1951).

25. Langmuir, I. and Blodgett, K. B., A Mathematical Investigation of Water Droplet Trajectories, Army Air Forces Technical Report No. 5418 (1946).

26. Lewis, H. G. et al, Ind. Eng. Chem., 40, 67 (1948).

27. Kolupaev, P. G., Sc. D. Thesis, M.I.T. (1941).

28. Schmidt, J. M., A Preliminary Investigation of the Atomization of Liquids Injected into an Air Stream, Jet Prop. Lab., Cal. Inst. Tech., Progress Report No. 4-101, May 23, 1949.

29. Longwell, J. P., et al, Preparation of Air-Fuel Mixtures for Ram-Jet Combustors, (Confidential), Standard Oil Development Co., Bumblebee Report No. 168, November 1951.

30. Dryden, H. L., Ind. Eng. Chem., 31. 416 (1939).

31. Taylor, G. I., Proc. London Math. Soc., 20, 196 (1921).

32. Taylor, G. I., Proc. Royal Soc. London, A157, 537 (1936); A151, 444 (1935).

33. Towle, W. L. and Sherwood, T. K., Ind. Eng. Chem., 31, 416 (1939).

34. Brown, H. E. and Yound, E. C., Droplet Dispersion Characteristics of Low Pressure, Disc Type Nozzles, The University of Texas, CM-618, July 3, 1950.

35. Brown, H. E. and Amstead, B. H., Droplet Dispersion in High Velocity Airstreams, Conference on Fuel Sprays, University of Michigan, March 30-31, 1949.

36. Standard Oil Development Co., Quarterly Report on Study of Combustors for Supersonic Ram-Jet for Period October 1 - December 31, 1950, (Confidential), CM-660, February 5, 1951.

37. Hardgrave, E. J., Jr. et al, Ordnance Aerophysics Laboratory, Consolidated Vultee Aircraft Corp., Daingerfield, Texas, Memo. 36, Add. 1, November 15, 1949.

38. Kennedy, E. C., Ordnance Aerophysics Laboratory, Consolidated Vultee Aircraft Corp., Daingerfield, Texas, Memo. 48, November 15, 1951.

39. Benedict, M. et al, Chem. Eng. Progress, 47, 571, 609 (1951).

40. Maxwell, J. B., Data Book on Hydrocarbons - Application to Process Engineering, Van Nostrand, 1950.

41. Godsave, G. A. E., The Burning of Single Drops of Fuel, Parts I and II, National Gas Turbine Establishment, Reports No. R66 (March 1950) and R87 (April 1951), Ministry of Supply, London.

42. Hirschfelder, J. O., Hydrodynamics of Gases, Chapt. IV, Univ. of Wisconsin, CF-1501, November 7, 1950.

43. Gilliland, E. R., Ind. Eng. Chem., 26, 681 (1934).

44. Langmuir, I., Phys. Rev., 12, 368 (1918).

45. Fuchs, N., Concerning the Velocity of Evaporation of Small Droplets in a Gas Atmosphere, Transl. in NACA TM 1150 (1947).

46. Bradley, R. S. et al, Proc. Royal Soc. of London, A186, 368 (1946); A198, 226, 239 (1949).

47. Stull, D. R., Ind. Eng. Chem., 39, 517 (1947).

48. Perry, J. H., Chemical Engineers' Handbook, Third ed., McGraw-Hill, 1950.

49. Probert, R. P., Phil. Mag., 37, Ser. 7, 95 (1946).

50. Ranz, W. E. and Marshall, W. R., Jr., Chem. Eng. Progress, 48, 141, 173 (1952).

51. Stewart, W. E., Sc. D. Thesis, M.I.T. (1950).

52. Tanasawa, Y. and Kobayase, K., Technology Reports of the Tohuku University, Japan, 14, No. 2, 55 (1951).

53. Ingebo, R. D., Vaporization Rates and Heat-Transfer Coefficients for Pure Liquid Drops, NACA TN 2368 (1951).

54. Hougen, O. A. and Watson, K. M., Chemical Process Principles, I, John Wiley and Sons, Inc., New York, 1953.

UNCLASSIFIED